Geochemical and petrological characteristics of the high-Fe basalts from the Northern Eastern Desert, Egypt: Abrupt transition from tholeiitic to mildly alkaline flow-derived basalts

Hatem M. El-Desoky [1], Ahmed E. Khalil [2], Atef A. Afifi [3]

[1] Department of Geology, Faculty of Science, Al-Azhar University, Egypt
[2] Department of Geology, National Research Center, Egypt
[3] Senior Researcher, Quarry Management, Cairo Governorate, Egypt
hatem_eldesoky@yahoo.com

Abstract: The Tertiary volcanism associated with continental rifting to the North Eastern Desert constitute a distinct anorogenic igneous rift assemblage of volcanic activity and is a part of widespread Phanerozoic igneous suites extending from the Nile Valley eastwards to the Gulf of Suez, and between Cairo-Suez railway and Cairo-Sukhna roads. The Mid Tertiary Volcanics occur as well-exposed extrusive sheets capping hills of Oligocene sands and gravels. Flow sheet shaped outcrops of within plate tholeiitic alkali basalts characterize the studied basaltic rocks. Geochemical data indicate that the basaltic rocks divided into three distinct varieties; alkaline basalts, sub-alkaline basalts, and tholeiitic basalts. Geochemically these basalts are alkaline to subalkaline. The alkaline character is confirmed by the discrimination P_2O_5 versus Zr and (Na_2O+K_2O) versus SiO_2 diagrams. Various discrimination diagrams of Zr/Y versus Ti/Y, Ti versus Zr and Zr versus Zr/Y confirm the within plate character of basalts. The tholeiitic nature is evident from FeO^t - (Na_2O + K_2O) – MgO and Al, ($Fe_{(total)}$ +Ti) and Mg plots. A slight negative Nb anomaly is present indicating characteristic continental tholeiite. They show depletion of Ni and Nb (ranges from 24 to 150 ppm and 10 to 127 ppm respectively). Regional geology and small negative Nb anomaly in the basaltic volcanic geochemistry suggest they were deposited in a stable continental Gulf of Suez rift environment. The geochemical characteristics of the basaltic rocks to most likely reflect variations in source characteristics, together with minor crustal contamination, rather than the process of volcanic-arc magmatism. The basaltic rocks represent fractional crystallization of olivine from a low-Mg basaltic magma. Compatible and incompatible trace element modelling suggests that all three-rock types probably originated from a lherzolite mantle source. Basaltic volcanism in the Northern Eastern Desert, Egypt underwent an abrupt change from low-K tholeiitic basalt and ferrobasalt to alkaline basalts.

Hatem M. El-Desoky, Ahmed E. Khalil and Atef A. Afifi. **Geochemical and petrological characteristics of the high-Fe basalts from the Northern Eastern Desert, Egypt: Abrupt transition from tholeiitic to mildly alkaline flow-derived basalts.** *Nat Sci* 2015;13(6):109-132]. (ISSN: 1545-0740). http://www.sciencepub.net/nature. 16

Keywords: Geochemistry, petrology, high-Fe basalts, Tertiary volcanism, Egypt.

Introduction

The study area lies southeast of Nile Delta occurs in the eastern part of Cairo that extends from the Nile Valley eastwards to the Gulf of Suez, and between Cairo-Suez railway and Cairo-Sukhna roads (Fig.1). These parts of Eastern Desert represent the unstable shelf units, which comprise the greater part of northern Egypt. This Mobile shelf shows tectonic disturbances, and as a result, structural highs and lows well represented in this area.

The studied area covered essentially of sedimentary rocks with limited basaltic flow sheets belonging to Tertiary and Quaternary periods. Basalts occur in the form of sheets near the top of the Oligocene sediments, underlie the marine Miocene sediments, and thus are consider as Oligo-Miocene in age. Basalts always connected with faulting and the fissures were avenues for the emanation. The stratigraphical position of the basaltic sheets along the whole Cairo-Suez district is in favor of assigning an Oligo-Miocene age to faulting.

The basalts of Anqabia and El-Yahmum form a succession of three distinct sheets, each with a characteristic field appearance. The three sheets are designate as lower sheet (A); middle sheet (B) and upper sheet (C). The lower and upper sheets are characteristically amygdaloidal and vesicular textures and mostly intensely altered. The middle sheet is massive, compact and mainly fresh (**El-Ashkar, 2002**).

The Oligocene deposits are widely distributed in the Cairo-Suez district. They cover a long tract of desert from northeast of Cairo to Anqabia, and form several patches to the south and north of the asphaltic road. The sediments are mainly composed of sand and gravel with large trunks and fragments of silicified wood and basalt flows and dykes (Fig.2).

The volcanic rocks are believed by different authors, to be Tertiary (Oligocene) and / or Mesozoic (Upper Cretaceous) ages, based on their field relations. Radiometric data based on the K-Ar methods, suggest a Lower Cretaceous age of 115 –

117 Ma for these rocks (**Meneisy and Kreuzer, 1974**). **Meneisy and Abdel Aal (1983)** after (**Issawi *et al*., 1999**) estimated the age of basalt as 22- 23 Ma (Late Oligocene and Early Miocene).

Several basalt flows reported in many localities in the Cairo – Suez district and Maadi – Qattamiya district. The largest basalt outcrops are at Gabal Abu Treifiya, Gabal El-Yahmum, Gabal Anqabia and Gabal Nassouri. At Gabal Gafra the basalt flow is 25m thick, in Anqabia area, it is about 17m thick, while at Abu Zabaal to the northwest of Cairo the thickness exceeds 60m (**Said, 1962; El-Hinnawi and Abdel Maksoud, 1972**).

The Gabal El-Nasuri basaltic flows are in the form of dykes, plugs cutting the Oligocene sands, and gravels along NE faults dissecting the area (**Shukri and Akmal, 1953**). According to **Foley (1941)**, the basaltic flows of this area reaching approximately a maximum thickness of 30 meters and it common in the western portion. **Tosson (1964)** stated that, the basalt of the Cairo-Suez area seems to belong to one phase of magmatic activity, for they are all stratigraphically and/or petrographically similar. In addition, they seem to have climbed along the faults that affected the area during the Oligocene time.

The present study aims to establish the geology, petrography, geochemistry and petrogenesis of the mid-Tertiary basaltic rocks.

Geologic Setting

The Oligo-Miocene basaltic flows of the study area form huge sheets of wide extension.

The **Gabal El-Yahmum** basaltic flows and plugs (dykes; Fig.2) have been erupted in Late Oligocene – Early Miocene times, along the planes and fissures, following the general fault trends of the study district. The basaltic flows overlie the Oligocene sediments and widely distributed in El-Yahmum area, especially in the eastern part. The huge quarry of basalt lies in the El-Yahmum area, where the basalt face measures more than 25m (Figs.3a & b). The fresh surface of the El-Yahmum basalt is black, hard, massive with feldspar phenocrysts. The Oligocene fluviatile sediments in the El-Yahmum area preserved in the topographically low hills, and disappeared on the crests of the topographical highs. Generally, the Oligocene sediments are mainly composed of loose white sands, varicolored sands and gravels with silicified wood at the lower parts. Sometimes they form hills of dark brown to black color. In some places, they are caped by basaltic flows.

The fresh basaltic rocks of **Naqb Ghul** area are dark grey in color, very fine-grained, massive and hard (Fig.3d). The thickness of the Oligocene sediments in the Wadi Naqb Ghul area is about 24-31m. Silicification and multiferrugination occur along fissures, joints and fault planes due to hydrothermal solutions accompanying the extrusion of basalt (Fig.4a). The weathered basaltic rocks are of pale grey color and friable due to the weathering processes. The Naqb Ghul Oligocene sediments are mainly composed of loose sand and gravel with large trunks of silicified wood. The Oligocene outcrops in the Northern Galala area represented by Gabal Ahmar sand and gravel and basaltic flows. The Gabal Ahmar rocks consist mainly of multicolored sand and gravel with silicified wood fragments. The Oligocene gravel forms dark brown and black low hills with a characteristic dark appearance (Fig.4a). The sediments exhibit cross stratification, which is highly illustrated by the changing of colors, viz; reddish brown, brownish yellow and black (Fig.4b). The sand and gravel are usually loose or weakly consolidated. Therefore, hard cement sandstone is common in certain places, especially near fault planes due to uprising silica and iron bearing fluids.

The basaltic flows at **Wadi Qattamiya** area overlie the Oligocene sediments along Maadi-Qattamiya road (Fig.4c). Gabal Ahmar Formation covered by thin basalt flows represent a volcanic phase during the Oligocene period. These basaltic flows are always associated with fault lines. The thickness of the basalt flows recorded in the Wadi Qattamiya area (Southwest Gabal Umm Rihiyat) ranges between 1m and 8m. The surface of basalt flows and plugs are always weathered and converted into clay minerals and iron oxides. Wadi Qattamiya basalts are very dark grey in color, fine-grained, massive with fractures and cracks and the hardness is moderately of the fresh samples (Fig.4c). Vesicular basalts are observed in some parts and occasionally amygdaloidal in others. The sediments truncated by the faults usually imparted by red, yellow and brown colorations because of staining by iron oxyhydroxides.

Altered basalts represented mainly by dykes, which cutting the early formed basaltic rocks (Figs.3c & Fig.4d). The field occurrence of these basaltic rocks is very complex, which shows simple fissure eruptions and semi-ring structures.

The viscosity of this basaltic magma reduced by the incorporation of vapor, this due to the presence of altered minerals and deuteric alteration processes. Field occurrence is clearly demonstrates that they are separation from the early formed basalts by a considerable span of time. The tectonic event is rejuvenation and opening of genuine fractures and fissures filled by glassy altered basalts.

Altered basalts are dark green or brownish green and fine-grained rocks as well as they may have poured as subaquous flows. These basalts may be marginally silicified, stand as high ridges, concentric and rounded bodies of different sizes (Fig.4d).

Petrography

Thirty-nine samples representing basaltic rocks from Gabal El-Yahmum, Wadi Qattamiya area (Gabal Umm Rihiyat) and from Wadi Naqb Ghul area (Northern Galala Plateau) along the Gulf of Suez studied petrographically in detail by using polarizing microscope.

The basalts from each of the three above-mentioned localities described and classified as follows: doleritic olivine basalts and tholeiitic olivine basalts occurred at Gabal El-Yahmum and Wadi Naqb Ghul, andesitic olivine basalts at Wadi Qattamiya area and altered basalts at the 3 localities.

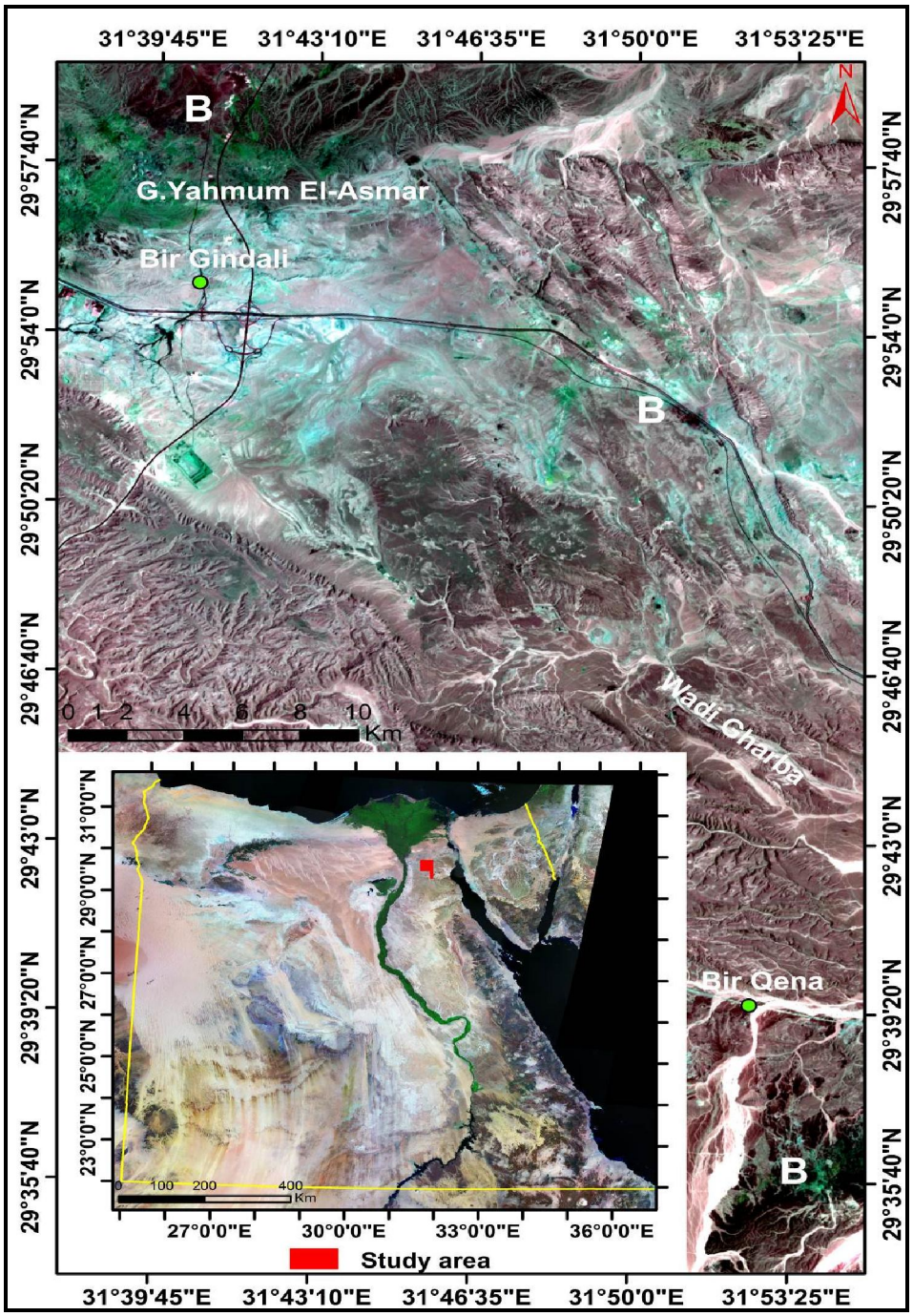

Fig.1. Showing false color landsat TM image (bands 1, 4, 3) of the studied area (B: Basalts).

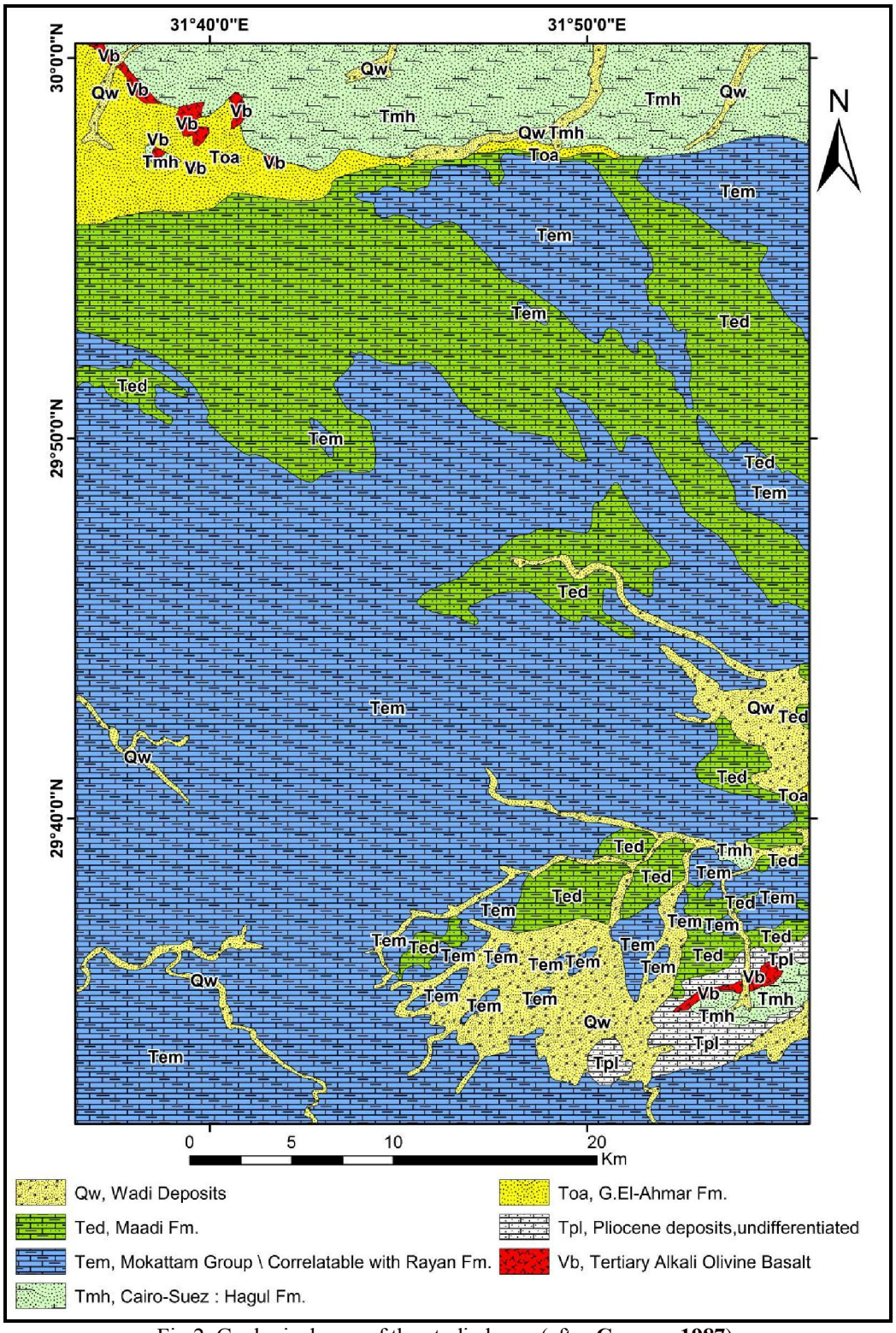

Fig.2. Geological map of the studied area (after **Conoco, 1987**).

1. Doleritic olivine basalts

The doleritic basalt is generally a porphyritic type with ophitic to subophitic and intergranular textures (Fig.5a). The plagioclase laths form doleritic and subdoleritic textures, depending on whether the intergranular spaces between them filled with crystals of olivine and pyroxene, or aggregates of both, respectively. It is fine- to medium-grained consisting

essentially of plagioclase, pyroxene (augite), olivine and iron oxides mainly magnetite.

Secondary minerals are subordinate including serpentine, chlorite and calcite. Iddingsite is a reddish-brown mixture of silicate minerals formed by the alteration of olivine (Fig.5b).

Plagioclase occurs as a subhedral prismatic crystals about 0.3 mm in length and 0.22 mm in width and arranged in a doleritic pattern. Plagioclase is generally fresh and sometimes slightly saussuritized. It is frequently zoned and well twinned, according to albite and combined albite-Carlsbad laws. Some plagioclase crystals may reach 3.5 mm long and induce the porphyritic texture for the rocks (Fig.5c). **Augite** forms anhedral crystals filling the angular interstices between plagioclase crystals. Augite is light green to brown color and encloses plagioclase laths forming ophitic and subophitic like intergrowths textures. Some pyroxene crystals are rich in the strongly colored pleochroic titanaugite. Titanaugite is appearing in varied shades of brown and purplish tints, thus denoting significant titanium content. Some pyroxene crystals show titanaugite rims observed rimming a green augite core.

a.

b.

c.

d.

Fig.3 (a-d). Field photographs of the studied basalts.

a. The basaltic flows overlie the Oligocene sediments in the eastern part of El-Yahmum area.
b. The huge quarry of the basalt face measures exhibit columnar joints and more than 25m lies in the El-Yahmum area.
c. Altered basaltic dykes cutting the early formed basaltic rocks in Gabal El-Yahmum area.
d. Thick basaltic flows overlie the Oligocene sand and gravel in the Northern Galala district (Naqb Ghul).

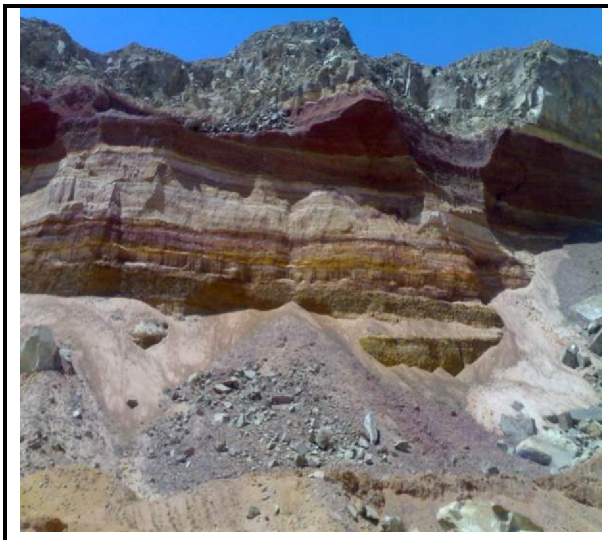

a.

b.

c.

d.

Fig.4 (a-d). Field photographs of the studied basalts.

a. The loose sand illustrated by the changing in colors as reddish brown, brownish yellow and black in Naqb Ghul.
b. The Oligocene sediments form dark red and brown colors with capping of basaltic flow in Naqb Ghul area.
c. A characteristic dark grey appearance of thick basaltic flow in Wadi Qattamiya area.
d. Complex fractures and fissures filled by glassy yellow altered basalts in Wadi Qattamiya.

Augite crystals are enclosing bladed plagioclases and giving the rock an ophimottled texture or speckled appearance (Fig.5a).

Olivine represents the least mode in the rock, apparently of early crystallization, being frequently mantled by the finely crystals of pyroxene indication of tholeiitic nature, and is usually serpentinized along the cracks. Olivine occurs as small anhedral to subhedral rounded crystals either enclosed in pyroxenes or aggregated within the intergranular spaces between plagioclase laths. The olivine altered to reddish-brown iddingsite along rims and sometimes is completely pseudomorphed by green fibrous chlorite (Fig.5b). Advanced stages of alteration of olivine is marked by the complete alteration to brown mineral, possibly a mixture of iron oxides in various stages of oxidation and hydration, (Fig.5d) associated with chlorite (**Fawcett, 1965**).

Iron oxides are mainly represented by irregular grains of magnetite, vary in size, and shape from large to small grains embedded in the olivine and pyroxene crystals (Fig.5d).

2. Tholeiitic olivine basalts (olivine tholeiites)

Tholeiitic olivine basalts contain both augite and low-Ca pyroxene (pigeonite and/or hypersthene). Olivine is present only in small amounts and these rocks contains varying amounts of interstitial brown glass (Fig.6a), or devitrified glass (intersertal texture); in more slowly cooled rocks, the place of the glass is taken by intergranular or subophitic texture. These rocks may be uniform in grain size or they may have microphenocrysts of plagioclase, augite and olivine.

Most Icelandic lavas are tholeiitic olivine basalts have about equal amounts of normative ol and hy (each ~ 10-12%; **Sigvaldson, 1974**; **Jakobssonet et al., 1978**).

These rocks consist essentially of plagioclase, augite and/or hypersthene and olivine, the two latter in smaller quantity. These basalts distinguished from the doleritic and andesitic olivine basalts by the occurrence of orthopyroxene (Fig.6b).

Plagioclase varies from slender laths to euhedral crystals that are 1 mm length and 0.3 mm width. The plagioclase shows lamellar and Carlsbad twinning (Fig.6c) and some crystals exhibit normal zoning with calcic core and sodic rims. Few crystals contain inclusions of iron oxides and veinlets of calcite (Fig.6d).

The **augite** varies in color from almost colorless to deep lilac in different rocks, depending on titanium content. It may be present as grains or as small ophitic or subophitic plates enclosing the plagioclase.

Hypersthene forms isolated crystals and less frequently aggregates that are in subophitic relationship to plagioclase laths. The characteristic pleochroism from green to pink is a good indication of the presence of hypersthene. Hypersthene usually occurs in subhedral crystals of prismatic habit.

Olivine sometimes partly altered to iddingsite, chlorite or serpentine, occurs as subhedral grains (Fig.6c). The **iron oxides** occur as anhedral to subhedral grains and also as irregular crystals and specks distributed between and within the other mineral constituents.

3. Andesitic olivine basalts

The andesitic olivine basalts differ from the doleritic olivine basalts in being porphyritic in texture with 51% phenocrysts (plagioclase, olivine and augite) and 49% groundmass (iron oxides, augite, plagioclase and volcanic ash). The rocks are fine-grained, plagiophyric basalts with a finer-grained groundmass. Some basalt is vesicular and amygdaloidal (Fig.7a). Amygdales filled with quartz, chlorite and calcite. The amygdales are few, rounded or irregular in shape and in some cases; they filled with pale yellow and brown fibrous minerals of the alteration products of olivine (Fig.7a). Phenocrysts of plagioclase and olivine, some in clots, are set in fine-grained ophimottled groundmass (Fig.7b). These basalts consist essentially of plagioclase, olivine, augite and iron oxides phenocrysts.

Plagioclase found as phenocrysts and as small crystals. The phenocrysts are euhedral to subhedral, sometimes well-developed prismatic crystals, exhibiting lamellar and Carlsbad twinning. Phenocrysts have an average of 0.96mm in length and 0.27mm in width while the small crystals developed in the groundmass. They are characterized by porphyritic, ophitic, subophitic and poikilitic textures. In the poikilitic texture, inclusions of iron oxides arranged randomly within the phenocrysts (Fig.7b).

Augite occurs as phenocrysts, granules and as small crystals in the groundmass. Augite is subhedral in crystal form and varies from pale brown to purplish brown in color. Sometimes, a titaniferous augite of brownish green color and faint pleochroism detected. Both glomeroporphyritic and porphyritic textures recorded in addition to ophitic and subophitic textures. Augite includes plagioclase crystals in ophitic and subophitic textures. Discrete phenocrysts of plagioclase, augite and olivine, and clots consisting of a few crystals of the same minerals, are set in a finer-grained groundmass, in places showing slight alignment of plagioclase needles. Some plagioclases in individual clots aligned-this arrangement is common in plagioclase glomerocrysts (Fig.7b).

Olivine forms small, rounded phenocrysts while its occurrence in the groundmass is rare. This indicates probable early formation of olivine. It partially altered along borders and cracks to reddish-brown iddingsite and green fibro-lamellar chlorite. The olivine altered on the periphery to iddingsite, magnetite and other iron oxides and on the cracks to serpentine and chlorite, iron oxides (mainly magnetite) from a black rim around the olivine crystal and sometimes occurs as pseudomorph after olivine.

The iron oxides present in vary size and shape from phenocrysts to small grains embedded in the groundmass.

Flotation of plagioclase crystals and sinking of augite and olivine may result in clustering of early formed crystal aggregates that impart glomeroporphyritic textures to tops and bottoms of thick flows and sills. (**Williams, *et al.*, 1985**). Some quartz is very rare in olivine basalts and may be is accompany olivine as xenocrysts picked up from sedimentary rocks or incorporated in basalts magma after sinking from overlying siliceous layers during the upraise of the magma.

4. Altered basalts

The altered basalts are composed essentially of numerous microlites and acicular crystals of plagioclase and augite, fine laths and grains of iron ore

minerals, and elongated grains of carbonates (calcite; Fig.7c).

The most common textures are spherulitic and porphyritic textures (Fig.7d). The spherulite consists of a dense mass of very fine intergrown needles of both plagioclase and augite radiating from a common nucleus. Spherulitic texture forms spherulitic fan-shaped aggregates up to 2.1 cm in size on altered basaltic lava (Fig.7d).

The spherulite comprises approximately some elongate crystals of ferro-pyroxene and plagioclase, each having a different optical orientation. Spherulitic pyroxenophyric basalts are composed of large spherical segregations of radially diverging prismatic clinopyroxene crystals found in altered basalts. The size of spherulites varies from 0.2 – 0.6cm, though are typically 1.2 – 2.1cm. Depending on the size, small (with diameters of spherocrysts 0.2 – 2.1cm) and large-spherulite (1.2 - 2.1 cm).

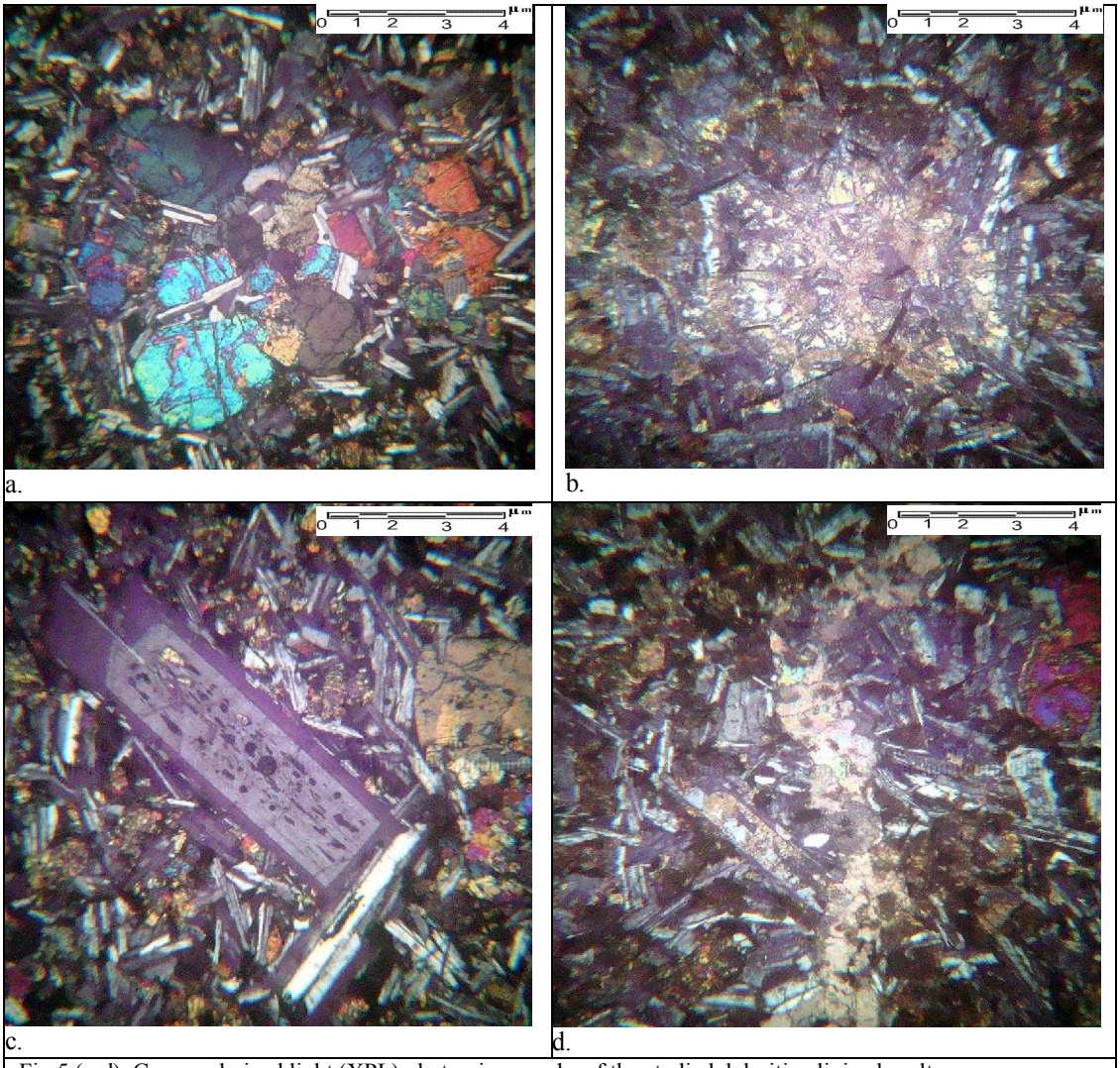

Fig.5 (a-d). Cross-polarized light (XPL) photomicrographs of the studied doleritic olivine basalts.
a. Ophitic and subophitic textures.
b. Iddingsite is the alteration of olivine.
c. The porphyritic texture of zoned plagioclase crystal.
d. The complete alteration of olivine to brown mixture of iron oxides in various stages of oxidation and veinlets of calcite.

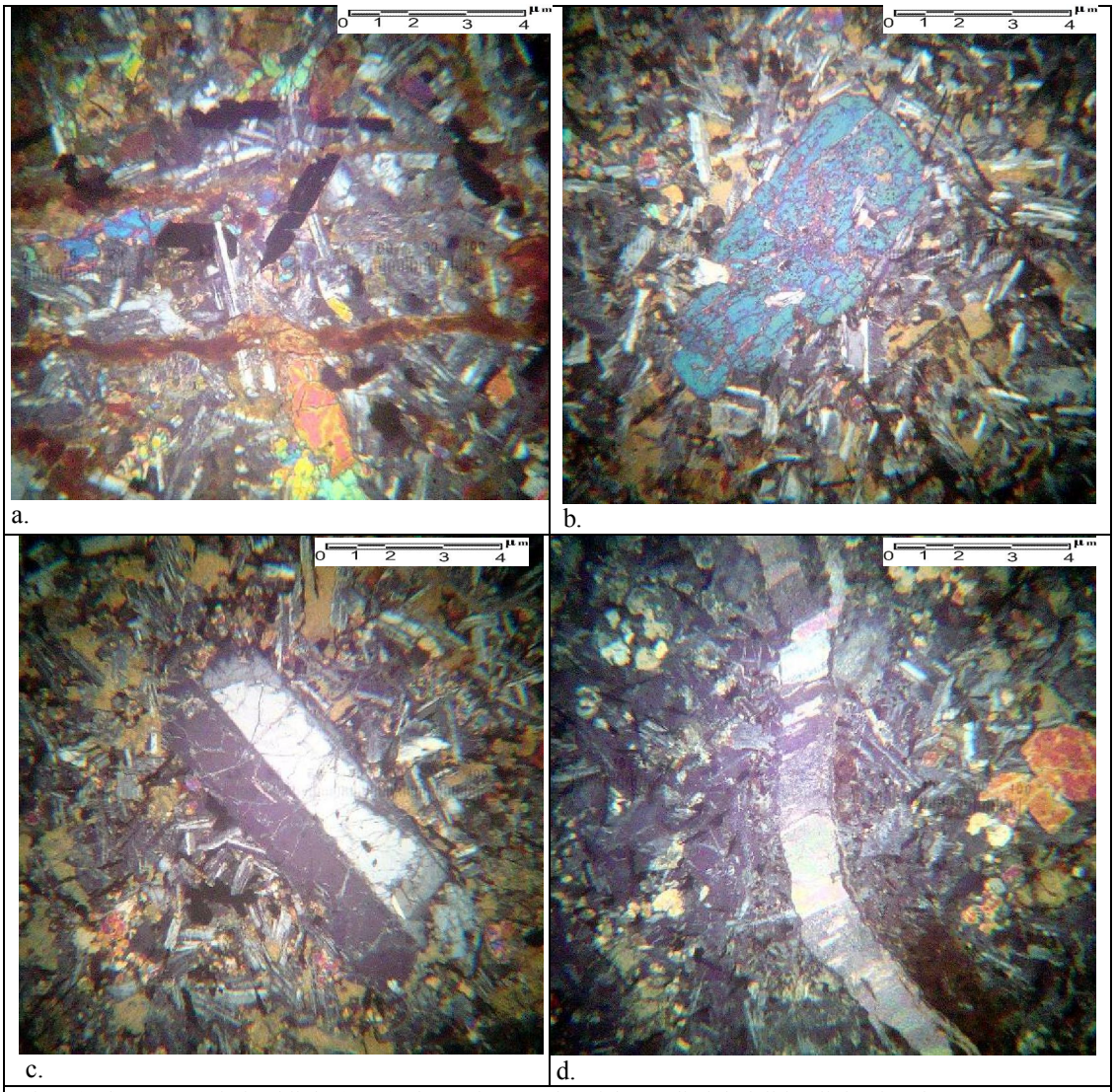

Fig.6 (a-d). Cross-polarized light (XPL) photomicrographs of the studied tholeiitic olivine basalts.
a. The tholeiitic olivine basalts contain varying amounts of interstitial brown glass.
b. The tholeiitic olivine basalts distinguished by the occurrence of orthopyroxene.
c. The plagioclase shows Carlsbad twinning and olivine partly altered to iddingsite or serpentine occurs as subhedral grains.
d. Microveinlets of calcite due to the complete alteration of plagioclase and pyroxene.

Mixed glassy and spherulitically devitrified zones

Most mafic units had thin, sparsely microlitic, glassy margins surrounding intensely microlitic cores. Mixed glassy and spherulitically devitrified zones originally comprised massive coherent volcanic glass with scattered spherulites and lithophysae, or bands of glass alternating with bands of spherulites and lithophysae, or a combination of both (Fig.7d).

Geochemistry

Thirteen analyzed rock samples representing the basaltic rocks of the three sites in the area under investigation. These samples chemically analyzed for major and trace elements where seven samples of doleritic olivine basalts (Gabal El-Yahmum), three samples of andesitic olivine basalts (Wadi Qattamiya), five samples of tholeiitic olivine basalts (Naqb Ghul and Gabal El-Yahmum) and two samples of altered basalts (Gabal El-Yahmum). The major and trace element concentrations of the studied basaltic rocks were presented in Table 1.

The average chemical composition of the basaltic rocks in the Egyptian volcanic districts and in the Earth and the Paleoproterozoic subalkaline volcanics are shown in Tables 2, 3 & 4.

Geochemistry of major and trace elements

The variation diagrams, for example the plot of MgO against major oxides and trace elements (Figs. 8, 9 & 10) discriminate two distinct geochemical trends

corresponding to the physicochemical processes that operated in the magmatic crystallization. Variations of trace elements are shown on figures (9 & 10). The three studied areas display similar trends for Cr, Ni, Cu, Co, V, Zr, Zn, and Y having decreasing contents with magmatic evolution. For Nb the opposite trend is manifested. The limited variations of incompatible trace elements in the studied rocks (Table 1) mainly reflect limited degrees of partial melting.

The major element compositions of basaltic rocks of the three examined occurrences are more or less similar. Their SiO_2 values vary between 27.26 wt.% and 48.05 wt.%; Al_2O_3 ranges from 0.60-16.96 wt.%; Fe_2O_3 ranges from 4.84-22.46 wt.%; FeO ranges from 1.02-15.73 wt.%; TiO_2 ranges from 0.11-3.97 wt.%; CaO ranges from 9.91-39.04 wt.% and MgO is between 0.56 wt.% and 3.86 wt.%.

The more primitive magma composition from the analyzed samples showing MgO content more than 3.5 wt.% and SiO_2 below 49 wt.%. The decreasing of K with SiO_2 increase may be due to a fractionation of potassic mineral phase that could crystallize early in water rich primitive melts.

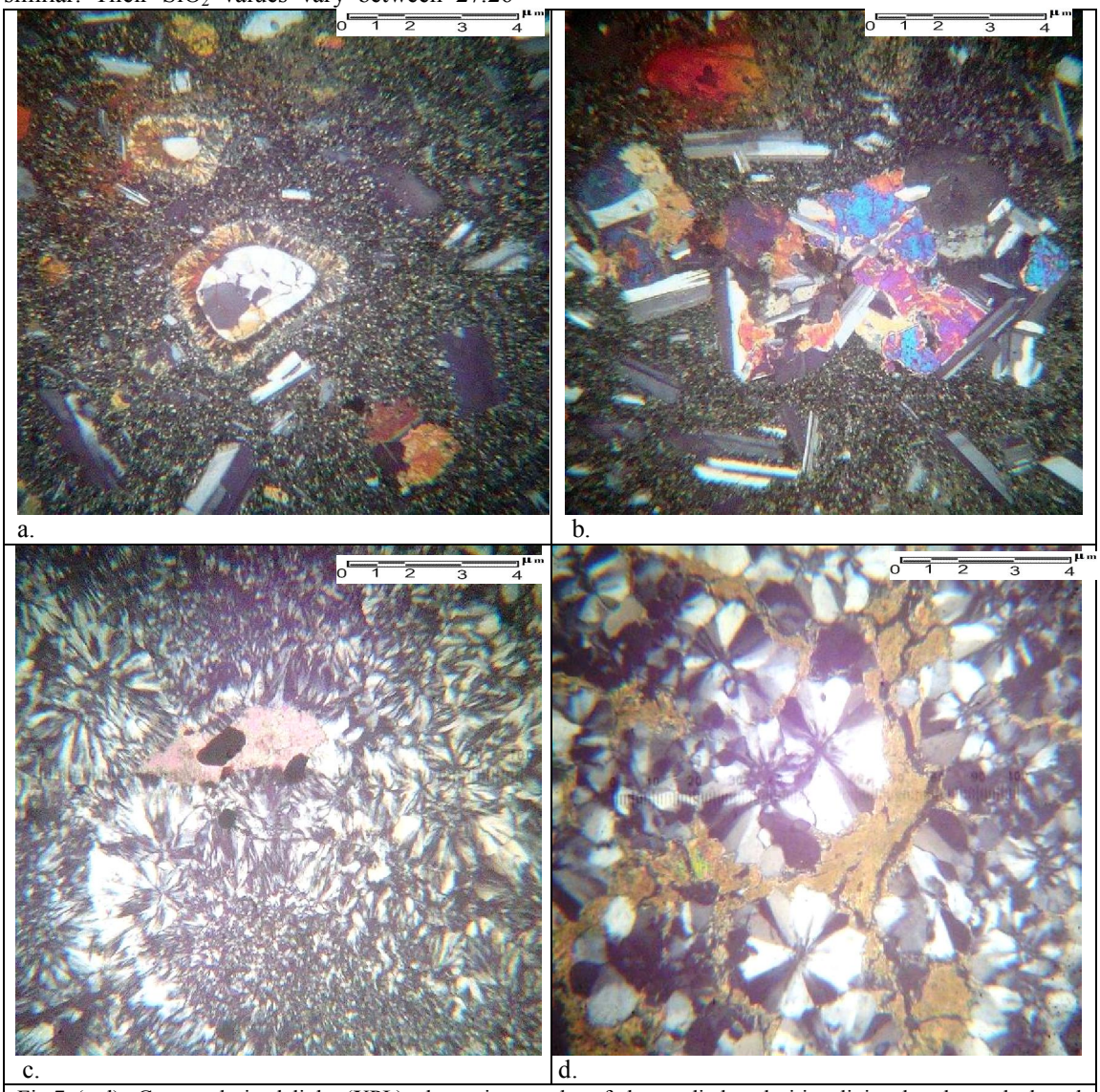

Fig.7 (a-d). Cross-polarized light (XPL) photomicrographs of the studied andesitic olivine basalts and altered basalts.

a. Amygdales are few, rounded or irregular in shape and filled with quartz and brown fibrous minerals of the alteration products of olivine.
b. Clots phenocrysts of plagioclase and olivine set in fine-grained ophimottled groundmass.
c. Numerous microlites of plagioclase and elongated grains of calcite.
d. Spherulitic and porphyritic textures in altered basalts.

Table 1. Chemical analyses of the major (wt. %) and trace elements (ppm) of the studied basaltic rocks.

Rock types	Doleritic olivine basalts							Andesitic olivine basalts			Tholeiitic olivine basalts					Altered basalts	
Oxides	1B	2B	3B	4B	5B	7H	10H	1Q	2Q	3Q	6B	6Nq	7Nq	8Nq	9Nq	8H	9HH
SiO_2	45.27	45.39	43.69	45.41	48.05	45.03	47.60	43.37	34.65	44.65	43.55	45.48	45.10	46.65	45.60	27.26	46.79
TiO_2	2.35	2.39	2.60	2.35	2.06	3.15	2.27	3.97	3.81	3.74	1.55	2.62	2.92	2.51	2.44	0.11	2.04
Al_2O_3	16.56	16.69	15.82	16.96	14.67	15.76	15.08	16.07	15.74	15.48	15.21	13.65	11.73	14.11	14.42	0.60	14.96
Fe_2O_3	5.55	5.47	5.81	5.44	5.49	5.23	4.84	5.14	6.60	12.05	7.59	16.64	13.48	13.71	14.66	22.46	15.90
FeO	11.28	11.14	12.38	10.76	10.36	10.37	11.41	11.56	15.73	4.65	13.78	5.76	11.01	1.95	2.25	5.47	1.02
MnO	0.26	0.27	0.27	0.26	0.22	0.18	0.26	0.25	0.36	0.15	0.26	0.18	0.25	0.21	0.13	0.71	0.28
MgO	3.39	3.53	3.41	3.43	3.08	2.58	3.26	3.31	3.25	3.22	2.68	2.49	2.20	2.91	2.82	0.56	3.86
CaO	10.76	10.55	11.26	10.53	10.26	11.40	9.91	11.93	12.67	11.22	10.19	10.09	10.43	10.26	10.38	39.04	9.97
Na_2O	1.89	1.78	1.76	2.14	2.06	2.04	1.44	1.97	2.20	1.85	1.72	1.58	1.13	2.35	2.45	0.46	2.53
K_2O	1.28	1.34	1.24	1.28	1.32	1.42	1.16	0.57	1.44	0.85	0.50	0.18	0.93	0.92	1.10	0.06	0.28
P_2O_5	0.46	0.50	0.39	0.51	0.53	0.55	0.43	0.54	0.30	0.51	0.54	0.53	0.50	0.35	0.45	0.02	0.62
SO_3	0.11	0.11	0.39	0.10	0.08	0.14	0.11	0.15	0.32	0.13	0.62	0.20	0.19	0.12	0.16	0.88	0.19
Cl	0.29	0.21	0.29	0.22	0.32	0.54	0.31	0.53	1.42	0.35	0.12	0.03	0.03	0.04	0.06	0.69	0.05
LOI	0.55	0.54	0.64	0.54	0.66	0.62	0.68	0.62	0.64	0.65	0.75	0.65	0.06	3.35	2.58	0.70	0.83
Total	99.99	99.90	99.94	99.94	99.16	99.00	99.13	99.98	99.13	99.50	99.06	99.32	99.95	99.44	99.51	99.02	99.30
Trace elements (ppm)																	
Cr	200	300	100	200	100	100	200	100	200	100	100	110	91	100	105	200	110
Cu	100	105	100	100	117	169	32	114	100	110	200	100	80	105	110	200	50
Ga	200	200	200	200	48	100	61	79	200	80	100	40	78	50	44	100	79
Nb	80	40	50	10	92	127	40	47	57	44	70	41	17	40	50	20	24
Ni	36	43	80	24	34	93	70	50	60	41	39	110	89	40	45	70	150
Pb	210	120	140	210	110	83	90	210	130	63	320	37	321	100	110	285	36
Sr	163	140	152	146	156	120	131	210	940	190	213	590	420	85	80	100	510
Y	300	117	200	400	120	127	200	89	59	200	100	40	55	530	560	133	40
Zn	120	128	140	142	133	150	170	189	128	80	241	130	88	45	50	160	88
Zr	101	150	107	200	100	127	250	200	150	159	119	390	290	125	120	179	340
V	310	510	500	300	491	520	354	310	220	210	450	423	421	360	375	377	417
Co	150	122	152	142	129	168	146	142	152	318	126	122	132	360	380	188	144
Ti	1.40	1.43	1.55	1.40	1.23	1.88	1.36	2.38	2.28	140	2.92	2.87	2.98	139	128	2.77	2.71

B= Gabal El-Yahmum huge quarry of basalts. H= Gabal El-Yahmum basaltic sheets.
Q= Wadi Qattamiya basaltic sheets. Nq= Wadi Naqb Ghul (Northern Galala Plateau).

Table 2. Average Chemical composition of some Egyptian basalt.

	After **Atia, (1978)**							After **Abdel Aal, (1981)**			
Oxides	Abu Zaabal	Cairo-Suez Road	Abu Rawash	Red Sea Coast	Gabal Qatrani	El-Bahnasa	Bahariya Oasis	El-Alawy El-Zurq	South Quseir	Abu Treifiya	El-Gafra
SiO_2	47.28	47.78	47.35	48.17	47.60	44.70	47.94	48.71	46.72	46.80	49.99
Al_2O_3	16.54	15.96	16.96	16.52	16.12	17.02	18.32	15.24	15.24	15.51	14.34
Fe_2O_3	7.08	4.45	7.33	3.47	4.44	7.44	5.58	4.77	4.77	5.16	5.02
FeO	4.40	8.97	4.29	7.68	8.22	5.33	1.95	7.71	9.00	8.10	7.46
MnO	0.14	0.19	0.10	0.17	0.14	0.19	0.08	0.18	0.23	0.28	0.23
MgO	5.40	5.50	5.44	5.94	5.97	5.94	6.27	5.17	6.21	6.02	6.13
CaO	9.57	9.96	9.23	10.02	9.72	10.07	8.02	10.20	9.83	10.17	9.34
Na_2O	2.66	2.62	2.23	2.64	2.46	2.77	3.11	2.63	2.75	2.85	2.70
K_2O	0.74	0.92	0.71	0.77	0.76	0.64	1.55	0.72	0.75	0.67	0.60
TiO_2	2.48	2.85	2.56	2.40	2.52	2.99	2.18	2.56	2.40	2.82	2.60
P_2O_5	0.38	0.46	0.38	0.38	0.36	0.42	0.64	0.23	0.25	0.34	0.33
CO_2	--	--	--	--	--	--	--	--	--	--	--
H_2O^-	--	0.52	--	0.79	--	1.59	2.21	0.85	0.33	0.55	0.66
H_2O^+	--	0.39	--	--	--	--	--	1.26	1.59	1.43	0.96
$H_2O^{\pm}$	2.30	--	2.42	--	0.69	--	--	--	--	--	--
LOI	1.41	--	1.02	0.65	0.90	0.44	2.18	--	--	--	--
Total	100.38	100.57	100.05	99.60	99.88	99.54	100.03	100.23	99.98	100.70	100.36

Table 3. Average chemical analyses of some basalt (**Bogatikov *et al*., 1981**).

Oxides	Olivine basalts	Basalt	Leuco-basalt	Hypersthene basalt	Subalkalic olivine basalt	Subalkalic olivine leucobasalt	Subalkalic leucobasalt
SiO_2	46-49	48-52	49-53	47-53	44-48	48.6-25	49-35
TiO_2	<2.5	<3.0	<1.5	<1.0	2-3.5	1-2	0.5-1.5
Al_2O_3	12-17	13-18	17-21	16-23	12-15	16-18	18-22
Fe_2O_3	0.5-11	1-8	0.5-6	2-6	11-13	9-11	6-9
FeO	4-14	4-11	3-8	5-8	--	--	--
MnO	0-0.3	0-0.4	0-0.3	0.1-0.25	--	--	--
MgO	7-15	5-7	3-7	4-8	6-13	5-6.6	2-5.5
CaO	6-13	6-13	7-13	8-11	8-11	7-9	7-9.5
Na_2O	1.5-3.5	1-3.5	2-2.5	2-3.5	1.5-4	5-4.2	4-5
K_2O	0.1-2	0-1.5	0.1-0.9	0.5-1.5	0.5-1.5	0.8-1.8	1.5-2.5
Na_2O/K_2O	>4.1-4	>4.1-4	>4	1-4	>4.1-4	>4.1-4	1-4

Table 4. Chemical analyses of some world basaltic rocks.

	After **Middlemost, (1985)**					The Paleoproterozoic subalkaline volcanics after **Srivastava, (2006)**					
Oxides	3	4	6	7	10	16	17	18	19	20	21
SiO_2	50.19	50.17	51.75	46.88	45.68	49.34	49.83	47.03	49.35	49.77	53.77
TiO_2	1.51	3.15	2.07	2.03	2.58	2.18	2.38	2.76	2.14	2.18	0.32
Al_2O_3	15.15	13.23	13.81	13.69	14.68	13.27	12.07	13.19	13.14	14.50	8.97
Fe_2O_3*	11.33	14.23	10.83	12.27	11.72	16.81	17.89	19.56	16.40	15.76	9.27
MnO	0.15	0.22	0.17	0.17	0.17	0.20	0.22	0.23	0.21	0.19	0.16
MgO	5.91	4.41	7.25	9.78	8.92	5.15	4.71	4.76	5.61	4.39	13.10
CaO	9.13	8.20	10.57	10.81	10.44	9.21	9.28	7.52	9.58	9.39	12.38
Na_2O	2.71	2.85	2.31	2.47	3.11	2.63	2.41	3.05	2.28	2.51	1.19
K_2O	0.62	1.26	0.42	0.68	1.30	1.19	0.71	0.77	0.80	1.11	0.21
P_2O_5	0.17	0.67	0.24	0.24	0.52	0.28	0.30	0.34	0.26	0.29	0.05
H_2O^+	1.92	0.85	0.19	-	0.87	-	-	-	-	-	-
CO_2	0.13	0.05	0.06	-	-	-	-	-	-	-	-
Total	98.92	99.29	99.67	99.02	-	100.26	99.80	99.21	99.77	100.09	99.42
Trace elements (ppm)											
Cr	124	34	350	30.1	26.2	99	58	70	114	64	1810
Sc	30.7	36.7	29.5	560	563	-	-	-	-	-	-

Th	2.8	4.18	0.56	1.20	4.5	-	-	-	-	-	-
Sr	184	301	344	359	842	162	126	176	147	164	80
Zr	150	-	129	166	213	183	172	162	169	190	37
Hf	4.5	5.37	3.48	3	6.36	-	-	-	-	-	-
Rb	8	33	6.9	15	40	79	44	26	43	60	4

3. Continental flood basalt from the Keweenawan lavas of the North Shore Volcanic Group, Minnesota, USA (BVSP 1981: 67, KEW-15).
4. Continental flood basalt from the Columbia River Province, USA (BVSP 1981: 82, CP-6, Roza Member of the Wanapum Basalt Formation).
6. Tholeiitic basalt from Mauna Loa Volcano, Hawaii, 1859 eruption (BVSP 1981: 166, HAW-4).
7. Alkalic basalt or alkali olivine basalt, Hualalai Volcano, Hawaii, prehistoric eruption (BVSP 1981: 166, HAW-12).
10. Mean chemical composition of alkaline basalt.

Some trace elements such as Cr, Ni, V, Sr, Zr, and Y also display similar trends. The decrease of Cr and Ni content could be related to the fractionation of olivine, clinopyroxene and spinel, while V has relation to Fe-Ti oxides.

High field strong element (HFSE) and other elements showing well-preserved igneous characteristics used to identify the crystallization behavior of the studied volcanic rocks. Figures (9 & 10) show variations of some trace elements plotted versus MgO. In all plots, samples from the different basalts plot separately and show different crystallization behavior. Gabal El-Yahmum samples show higher concentrations of high-field strength elements (HFSE) than the Naqb Ghul samples. The most important observation is that different HFSE contents similar MgO (0.56 – 3.86 wt.%). This observation clearly suggests that samples from the subalkaline basaltic magmas. On the other hand, Wadi Qattamiya samples plot separately from the subalkaline samples suggesting different origin.

In general, HFSE concentrations increase with decreasing MgO in samples from all four basalt types and follow different crystallization trends. These observations are further corroborated on the variation diagram of SiO_2, TiO_2, Al_2O_3, Fe_2O_3 and CaO (Figs. 8 & 9).

Geochemical Classifications

Relative to most common igneous rocks, basalts are rich in MgO and CaO and low in SiO_2 and the alkali oxides; therefore, $Na_2O + K_2O$, consistent with the total alkali silica (TAS) classification. The **Cox *et al.* (1979)** diagrams (Fig.11a & b) place the studied basaltic rocks in their appropriate fields. The basalts plot in the basalt fields; these exactly conform to petrographic studies.

The **Middlemost (1980)** diagram (Fig.11c) shows that most of the basaltic rocks cluster between the alkalic basalt and sub-alkalic basalt fields and in transitional basalts. The basaltic rocks on **Le Maitre (2002)** diagram stretch between the basanite and basalt field (Fig.11d).

Tholeiite-alkaline nature

The alkaline and tholeiite nature of the studied basalts is depicted on the various plots of P_2O_5 – Zr diagram (**Floyd and Winchester, 1976)**, TiO_2 – Y/Nb diagram (**Floyd and Winchester, 1975)**, Al - ($Fe_{(total)}$ + Ti) - Mg diagram (**Rickwood, 1989)**, and total alkalis against silica **(Kuno, 1966 & Tegyey, 1974)**.

The **Floyd and Winchester (1975 & 1976)** plots (Fig.12a & b), **Rickwood (1989)**, and **Kuno (1966) & Tegyey (1974)** diagrams (Fig.12d) enable all the studied basaltic rocks plot in the alkaline basalts, continental tholeiite (Fig.12d), and high-Fe tholeiite basalt fields (Fig.12c).

Magma Type

Figure (13a) showing the relationship between the basicity index {(Fe_2O_3 + FeO + ½ (MgO + CaO)} and alkali metals (**Church, 1975**). On this diagram, the plots of the chemical analyses occupy the field of basalts. These results confirm with data of the chemical analysis fall in the basalt field.

On the total alkali silica variation diagram (Fig.13b) of **Irvine and Baragar, (1971),** the rocks plot clusters on the boundary between the fields of the alkaline and sub-alkaline basalts. On FeO_t - (Na_2O + K_2O) - MgO diagram (Fig.13c) after **Irvine and Baragar, (1971)** "tholeiites" character dominates. The AFM diagram (Fig.13c) demonstrates that all the samples have a Fe enrichment trend and plot in the tholeiitic field, this due to the high Fe type of fractionation (**Kuno, 1968**).

A potassic and soda series character exhibited when plotted on the K_2O versus Na_2O diagram (Fig.13d) after **Middlemost (1975**). All the analyses have low potassium and relatively high sodium contents. The data thus indicates that the rocks are generally low in K_2O.

Tectonic Setting Evolution

The Tertiary volcanic continental margins of Britain and Greenland caused by opening of the North Atlantic in the presence of the Iceland plume. The Paraná and parts of the Karoo flood basalts together with volcanic continental margins generated when the South Atlantic opened. The Deccan flood basalts of India and the Seychelles-Saya da Malha volcanic province created when the Seychelles split off India above the Réunion hot spot. The Ethiopian and Yemen Traps created by rifting of the Red Sea and Gulf of Aden region above the Afar hot spot. The oldest and probably originally the largest flood basalt province of the Karoo produced when Gondwana split apart. New continental splits do not always occur above thermal anomalies in the mantle caused by plumes, but when they do, huge quantities of igneous

material are added to the continental crust. This is an important method of increasing the volume of the continental crust through geologic time (**White and McKenzie, 1989**).

Continental rifting during the dispersal of the supercontinent Pangaea was often accompanied by massive magmatism as evidenced by the frequent occurrence of flood basalts and thick igneous crust emplaced along a number of rifted margins (**White & McKenzie 1989**; **Holbrook & Kelemen 1993**; **Coffin & Eldholm 1994**).

The rifting of Arabia from Africa in the Afar depression is an ideal natural laboratory to address this problem since the region exposes subaerially the tectonically active transition from continental rifting to incipient seafloor spreading. We review recent constraints on along-axis variations in rift morphology, crustal and mantle structure, the distribution and style of ongoing faulting, subsurface magmatism and surface volcanism in the Red Sea rift of Afar to understand processes ultimately responsible for the formation of magmatic-rifted continental margins (**Keir, *et al*., 2013**).

These regional geological observations suggest a Phanerozoic continental rift environment in the north Eastern Desert of Egypt. Several discrimination diagrams, exclusively based on incompatible trace elements, have been used to infer possible tectonic setting for the studied basaltic volcanics.

The **Pearce *et al.* (1977**) plot (Fig.14a) clusters most of the studied basaltic rocks between the continental basalts (5) and spreading centre island (1) fields.

When TiO_2 is plotted against K_2O and P_2O_5 (Fig.14b) after **Pearce *et al.* (1975**) more than 90 % of the basalts samples from Gabal El-Yahmum and Naqb Ghul fall within the field of continental basalts, while a few samples of Wadi Qattamiya basalts fall in the tholeiitic basalt field. This may be due to the high contents of TiO_2 observed in these basaltic rocks (Fig.14b). Some of the samples display an oceanic affinity. This may be a result of abortive attempts to generate new sea floor by rifting, i.e. they related to a major flexture or tensional feature contemporaneous with the opening of the Red Sea (**Abdel Aal, 1998**).

The studied basaltic rocks fall in the field of "plateau volcanics" setting (Fig.14c; **Chandrasekharam and Parthasarathy, 1978** in **Al Malabeh, 1993**). **Pearce and Gale (1977)** used Ti, Zr and Y ratios to determine the tectonic environment of the basalts. By using these elements, they distinguished plate margin basalt and within plate basalt. Majority of the studied basalts falls in the field of within plate basalt to plate margin basalt (Fig.14d). **George (1985)** suggested that enriched trend on the Ti-Zr plot is a result of fractionation.

Majority of the studied basaltic rocks fall in the fields of within plate basalts to volcanic-arc basalts when Ti plotted against Zr (Fig.15a) after **Pearce and Cann (1973**). On the tectonomagmatic discrimination Zr/Y versus Zr diagram (Fig.15b) of the **Pearce and Norry (1979),** the majority of the samples fall in within plate basalt setting. Seven samples fall out side the diagram-designated fields showing enrichment of Zr.

On the K - Ti diagram (Fig.15c) after **Lutz (1980**), the Naqb Ghul and Gabal El-Yahmum basaltic flows follow the trend of the basalts from continental rifts. Three samples of Wadi Qattamiya basaltic flow follow the trend of the oceanic basalts due to the high values of Ti in this area.

Tholeiitic basalts generally related to four tectonomagmatic environments. The within-plate types comprise oceanic island basalts and continental basalts; the remainder includes margin types occurring as subduction zone basalts and oceanic-ridge and floor basalts. The V-Ti diagram (Fig.15d) of **Shervais (1982**) illustrate that samples of the Naqb Ghul and Gabal El-Yahmum basaltic flows show a within-plate tholeiitic nature while Wadi Qattamiya basaltic flow samples fall in the field below line Ti/V=100. This may be due to the low contents of V observed in these rocks.

Magmogenesis and magmatic evolution

Continental regions contain an enormous diversity of environments and volcanic products. The high pressure and CO_2-rich volatiles produce alkali basalts, whereas low pressures and H_2O-rich volatiles produce tholeiitic varieties (**Yoder, 1976**). The variations in minor and trace elements found in the different basaltic rocks may generally be attributed to (a) differing proportions of the major phases in the parental source rocks; (b) the degree of partial melting; (c) the nature of melting process (batch melting, fractional melting, zone melting or disequilibrium melting); and (d) the abundance of various minor phases (**Middlemost, 1985**). It is concluded that most of the primary sub-alkalic basaltic magma generated on Earth resulted from partial melting of normal upper mantle materials.

Tarney and Weaver (1987) pointed out that it is very difficult to distinguish the effects of crustal assimilation from contamination that may have been inherited from a mantle source affected by sediment subduction or contamination by subduction zone fluids.

Source rocks of the basalts for the partial melts probably include both peridotite and pyroxenite and the plate tectonic processes introduce basaltic crust into the peridotitic mantle (**Sobolev *et al*., 2007**). Partial melts of this hybrid pyroxenite are higher in

nickel and silicon but poorer in manganese, calcium, and magnesium than melts of peridotite.

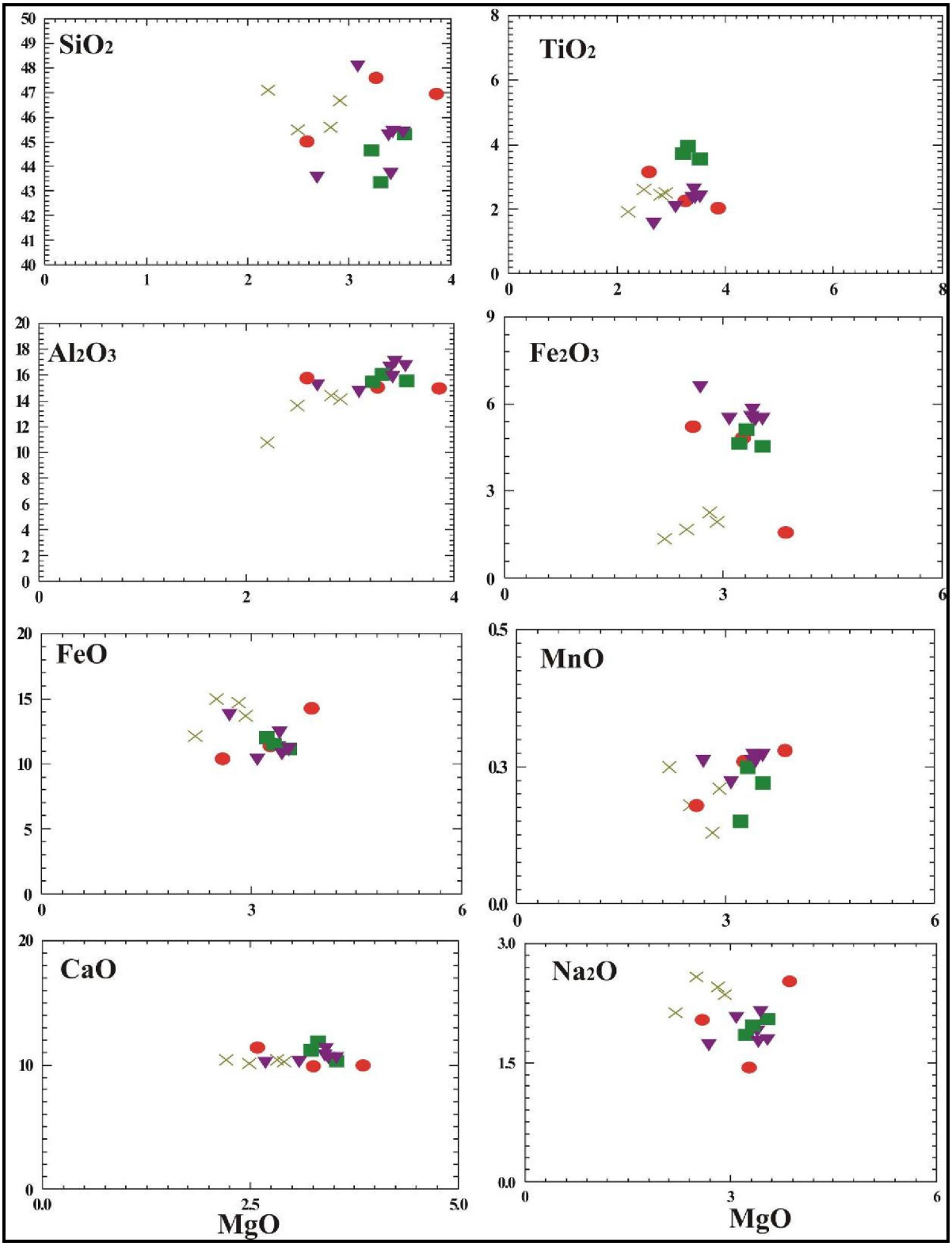

Fig.8. MgO variation diagrams for basaltic rocks: SiO_2, TiO_2, Al_2O_3, Fe_2O_3, FeO, MnO, CaO, and Na_2O. Symbols as in Fig.11a.

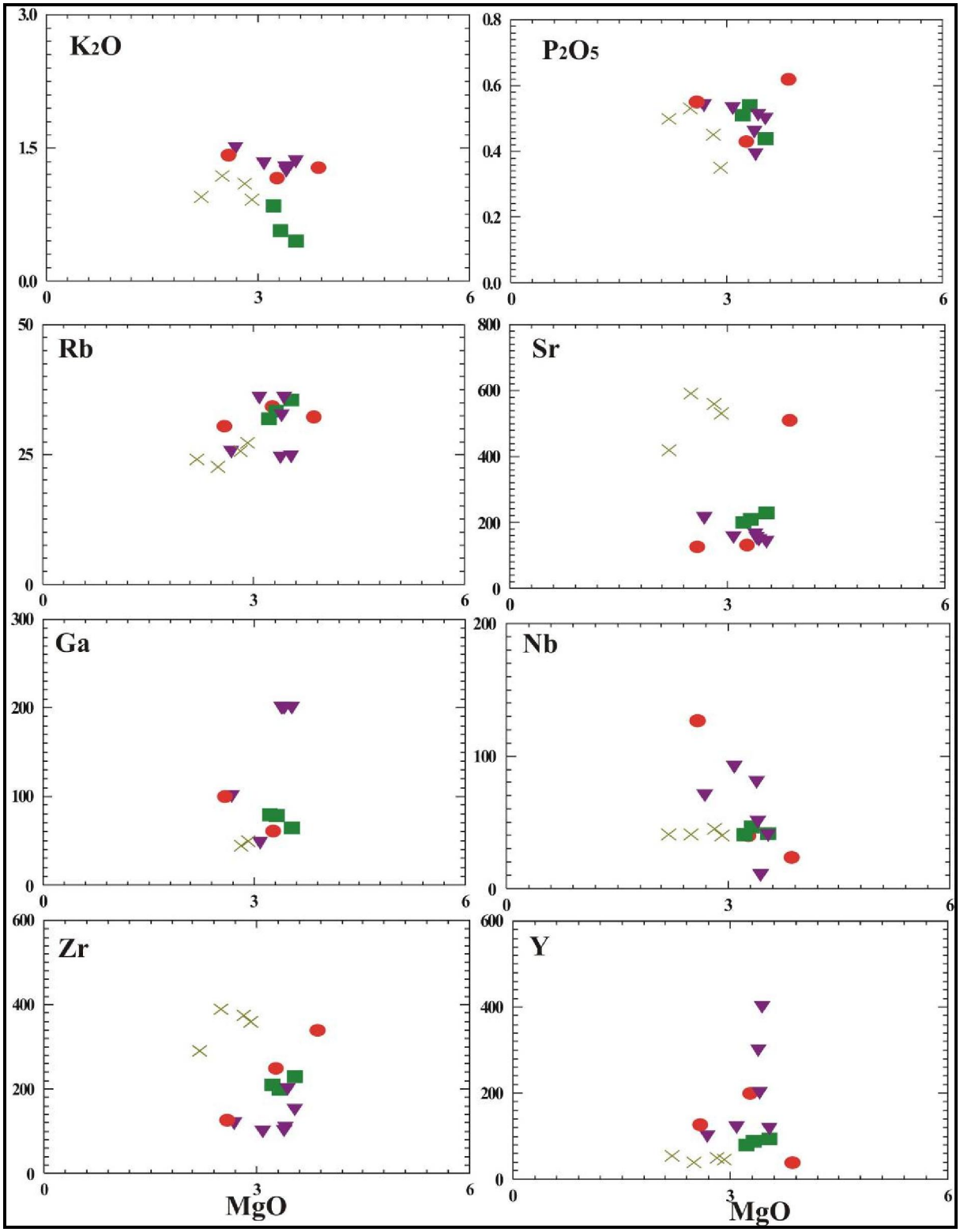

Fig.9. MgO variation diagrams for basaltic rocks: K_2O, P_2O_5, Rb, Sr, Ga, Nb, Zr, and Y. Symbols as in Fig.11a.

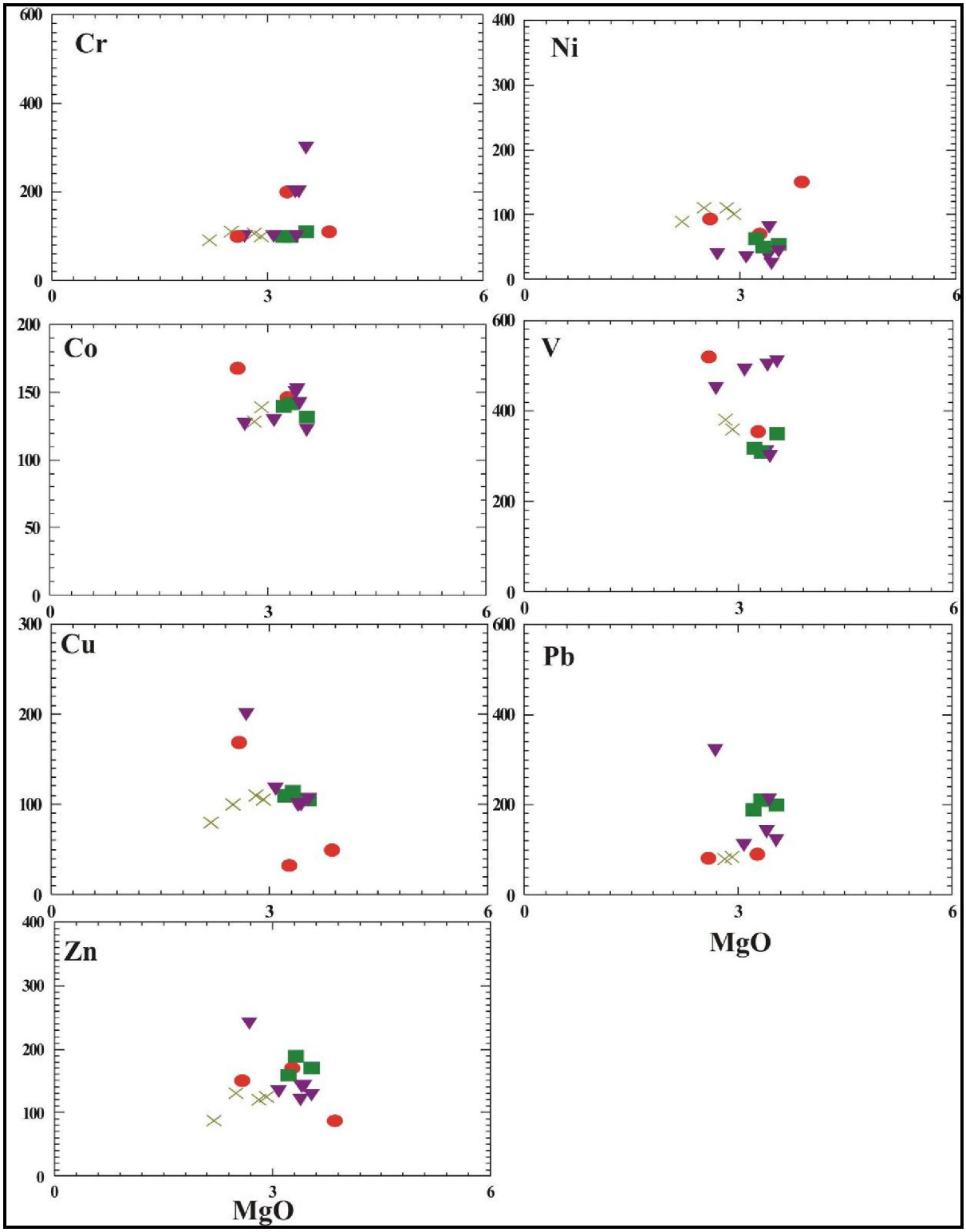

Fig.10. MgO variation diagrams for trace elements (ppm) in basaltic rocks: Cr, Ni, Co, V, Cu, Pb, and Zn. Symbols as in Fig.11a.

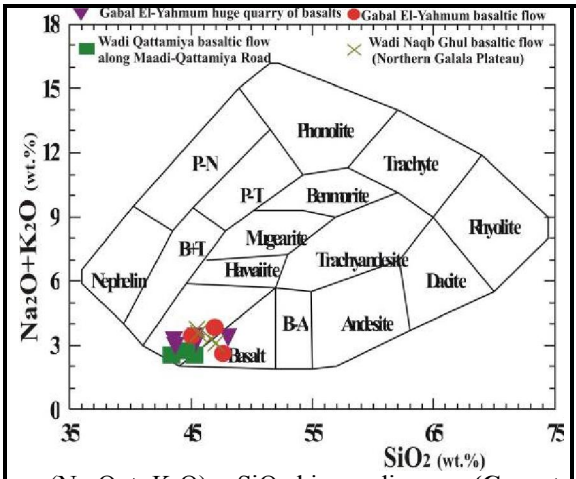

a. (Na_2O + K_2O) - SiO_2 binary diagram **(Cox *et al.*, 1979)**.

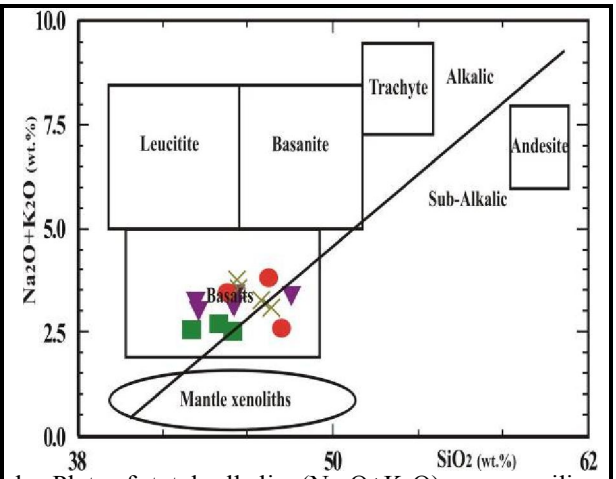

b. Plot of total alkalis (Na_2O+K_2O) versus silica (SiO_2), **(Cox *et al.*, 1979)**.

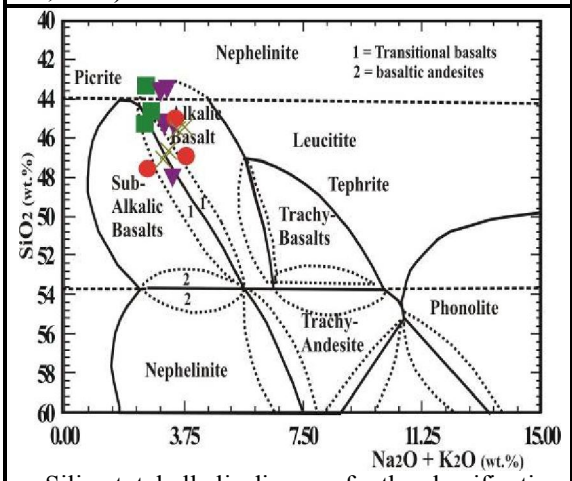

c. Silica-total alkalis diagram for the classification of basalts (**Middlemost, 1980**).

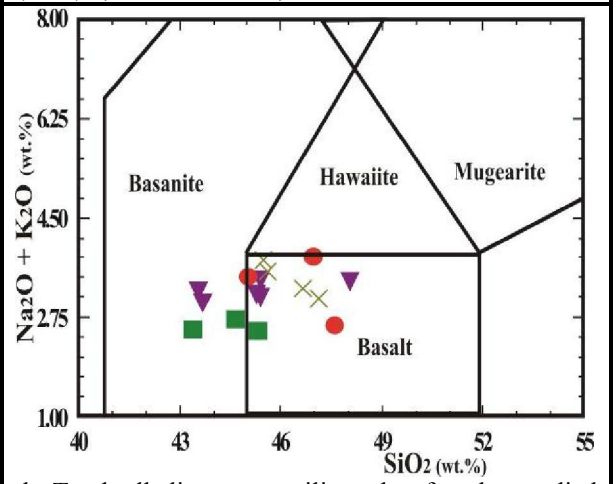

d. Total alkalis versus silica plot for the studied basalts **(Le Maitre, 2002)**.

Fig.11 (a-d). Geochemical classification diagrams of the studied basaltic rocks. Symbols as in Fig.11a.

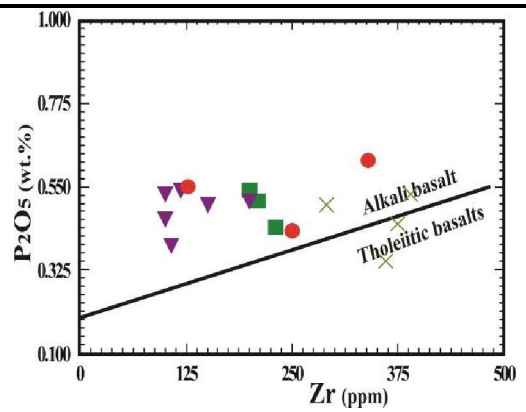

a. The P_2O_5 – Zr discrimination diagram for basalts **(Winchester and Floyd, 1976)**.

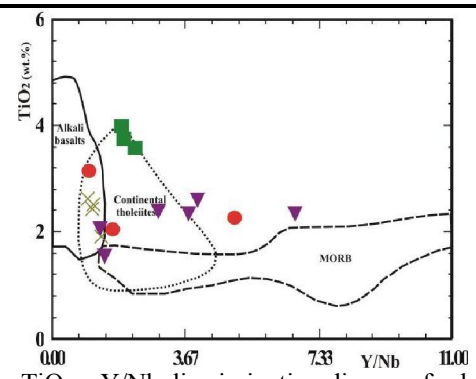

b. The TiO_2 – Y/Nb discrimination diagram for basalts (adapted from **Floyd and Winchester, 1975)**.

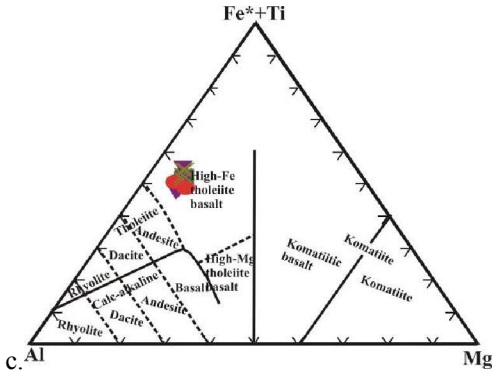

c. The classification of basaltic rocks according to their cation percentages of Al, ($Fe_{(total)}$ +Ti) and Mg showing the tholeiite, calc-alkaline and komatiite fields (**Rickwood, 1989**).

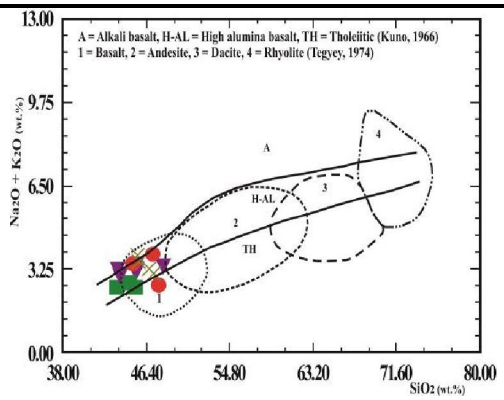

d. Plot of total alkalis against silica for the studied basalts **(Kuno, 1966 & Tegyey, 1974)**.

Fig.12 (a-d). Geochemical classification diagrams based on the magmatic nature for the studied basalts. Symbols as in Fig.11a.

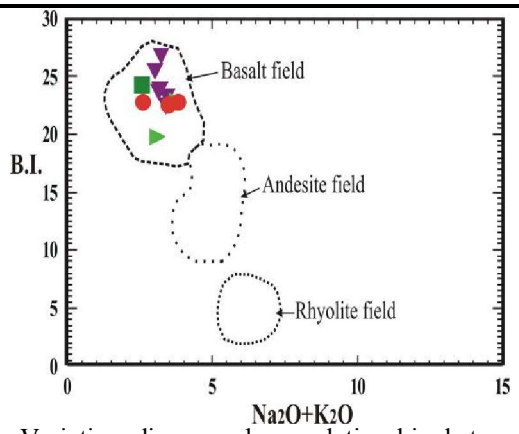

a. Variation diagram show relationship between basicity index and alkalis **(Church, 1975)**.

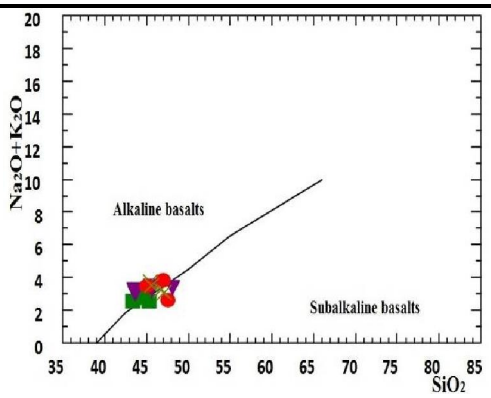

b. Total alkali silica variation diagram **(Irvine and Baragar, 1971)**.

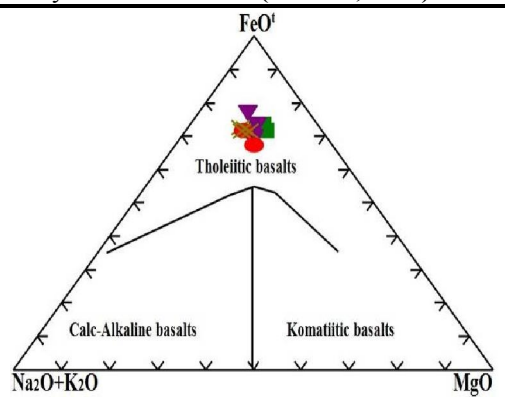

c. FeO_t - (Na_2O + K_2O) - MgO ternary diagram **(Irvine and Baragar, 1971)**.

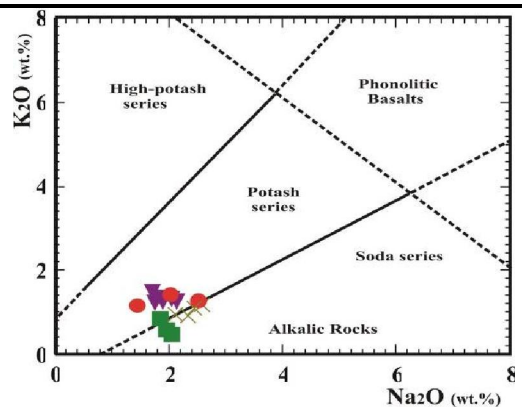

d. Potash versus soda variation diagram **(Middlemost, 1975)**.

Fig.13 (a-d). Geochemical diagrams showing the magma type of the studied basalts. Symbols as in Fig.11a.

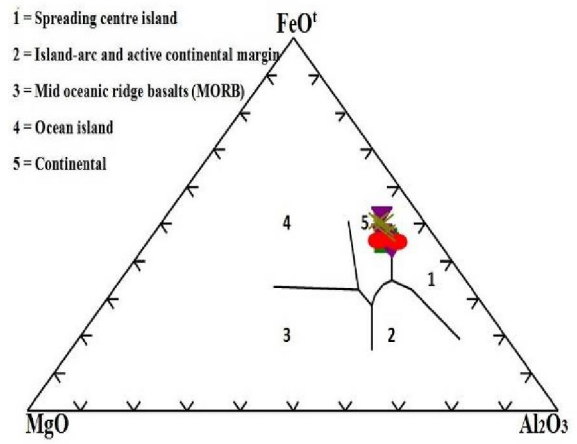

a. The $MgO-FeO^t-Al_2O_3$ diagram showing the tectonic settings of the studied basalts **(Pearce *et al.*, 1977)**.

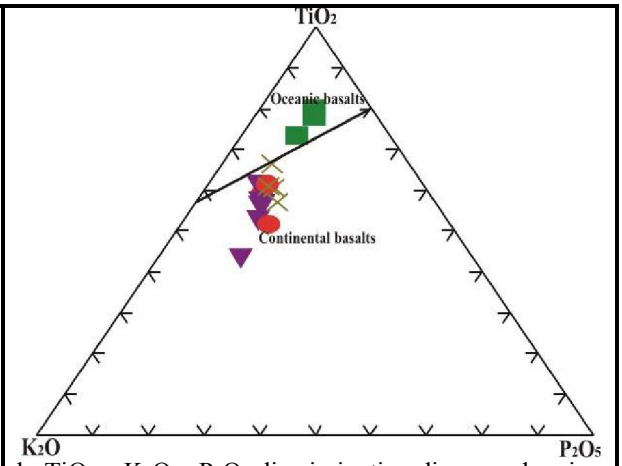

b. $TiO_2 - K_2O - P_2O_5$ discrimination diagram showing plotting of the studied basaltic samples **(Pearce *et al.*, 1975)**.

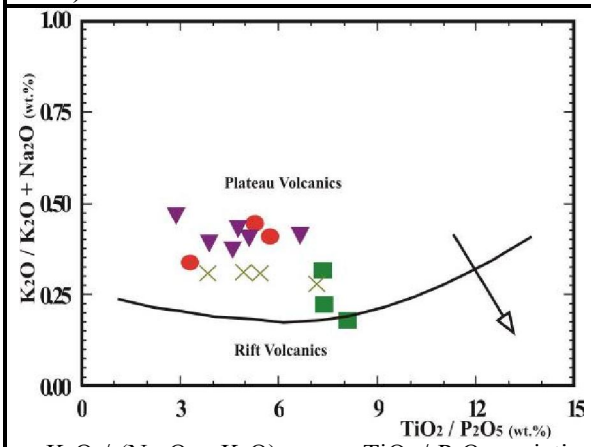

c. K_2O / (Na_2O + K_2O) versus TiO_2 / P_2O_5 variation diagram after **Chandrasekharam and Parthasarathy (1978)** in **Al Malabeh (1993)**.

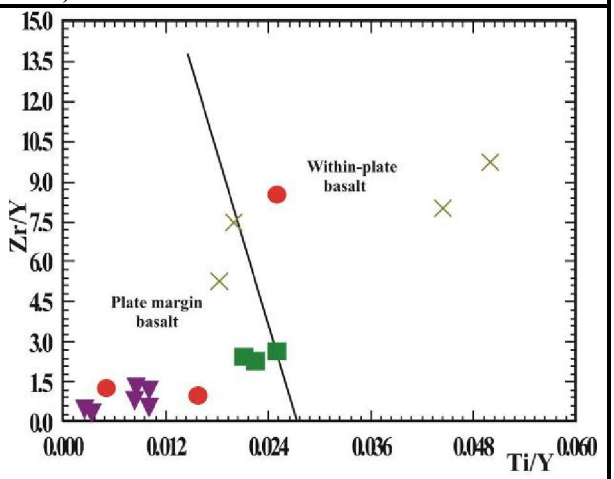

d. The Zr/Y – Ti/Y discrimination diagram for basalts (**Pearce and Gale, 1977**).

Fig.14 (a-d). Geochemical diagrams showing the tectonic setting types of the studied basalts. Symbols as in Fig.11a.

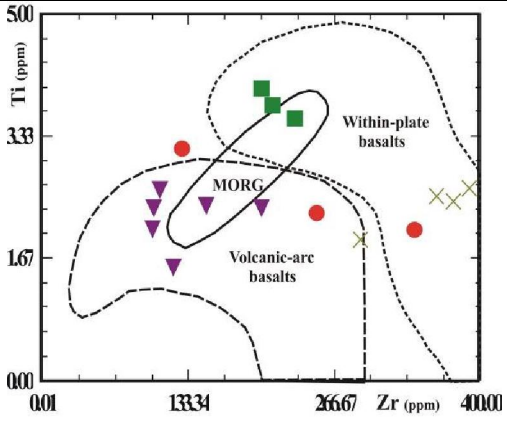

a. Discrimination diagram for basalts based up on Ti – Zr variation (**Pearce and Cann, 1973**).

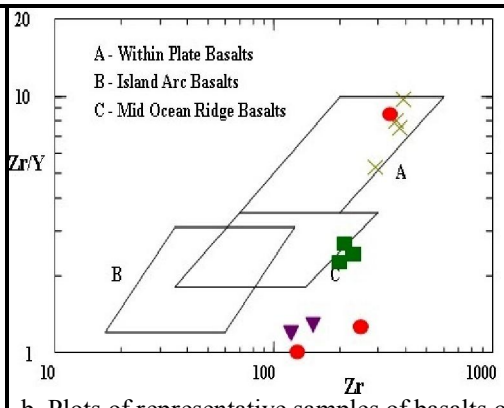

b. Plots of representative samples of basalts on the Zr versus Zr/Y diagram (**Pearce and Norry, 1979**).

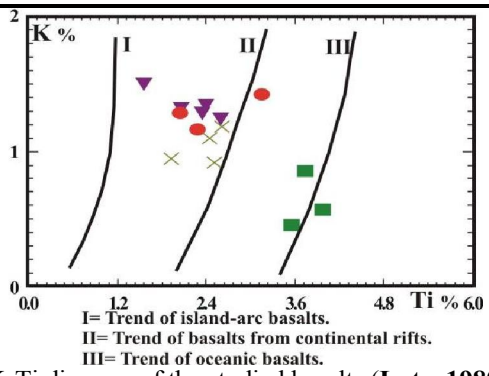

c. K-Ti diagram of the studied basalts (**Lutz, 1980**).

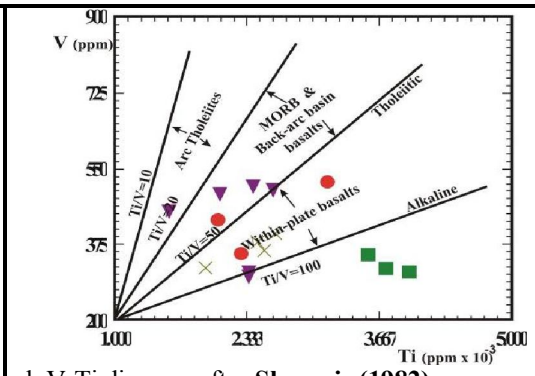

d. V-Ti diagram after **Shervais (1982)**.

Fig.15 (a-d). Geochemical diagrams showing the tectonic setting types of the studied basalts Symbols as in Fig.11a.

Mantle-derived magmas may be affected by some degree of crustal contamination during their ascent through, and/or temporary residence in crustal magma chambers (**Mohr, 1987**) within continental crust, and this is often invoked to explain the high concentration of LILE in continental flood basalts (**Cox and Hawkesworth, 1985**; **Campbell, 1985**). Wide variations in LILE are also observed for the studied basaltic rocks (Fig.16a & b).

The spiderdiagram plot (Fig.16a-b) shows the level of enrichment of the incompatible trace elements. The trough on K could be due to a refractory accessory phase like chlorite retaining it in the mantle. The trough on Ti could be attributed to its high mobility during upper mantle metasomatism.

Rajamani *et al*. (1985) suggested that a rock suite generated from different degrees of melting of the same source should have similar trend to melting curves presented in Figure (16c). Most of the studied samples fall on the batch-melting curve II (1250°C) and suggest about 10 and 20% melting of source material consistent with an origin as fractionation products. In binary plot of Zr versus Ni (Fig.16c), samples show less variation in Ni contents with increasing of Zr abundances indicating olivine-plagioclase fractionation (**Rajamani *et al*., 1985**). Compatible and incompatible trace elements modeling have been successfully used to understand conditions for generation of different mafic magmas in the upper mantle and to decipher their different processes (**Rajamani *et al*., 1985**; **Condie *et al*., 1987**; **Knoper and Condie, 1988**). Two of such models based on Zr – Ni (**Rajamani *et al*., 1985**), are used for the present mafic rocks (Fig.16c). This model indicates that basaltic rocks exposed in the northern Eastern Desert were probably derived from a low-magnesium mafic melt generated through ~5% batch melting of a depleted mantle source followed by 20-30% fractional crystallization. On the MgO - FeO* diagram (Fig.16d) of **Wood (1978)**, the rocks are considered as low Mg basalts.

Melting begins when upwelling mantle intersects the peridotite solidus. With decreasing P above the solidus, extent of melting increases. The amount of melting is limited by the heat available since the heat of fusion is large. Extent of melting can vary from ~1% to ~20%. The T, P, % melting, composition and mineralogy of source region, and presence and types of volatiles present determine the composition of the basaltic magma produced (Figs.17 & 18).

Discussion

The first evidence of Tertiary rifting that led to the present-day expression of the Gulf of Suez is manifest by Oligocene-Miocene basaltic volcanism and in poorly age-constrained, continental to shallow-marine clastics of the Abu Zenima and Nukhul formations (**Patton *et al*., 1994**).

The basalts occur mainly as fissure-erupted flows, associated with the pre-Miocene fault systems, which acted as channels for the magma. Both the fault system and the volcanic activity seem to be genetically connected with a regional Mid to Late Tertiary tensional phase that resulted in both the initiation and reactivation of the dominant fault system with east-west and northwest-southeast trends, and also in the eruption of the simatic magma that flooded northern Egypt during the Mid to Late Tertiary (**Abdel Aal, 1998**).

The northwestern Red Sea and Gulf of Suez rift system was initiated during Late Oligocene time and underwent extension in a N65°E direction, almost orthogonal to pre-existing WNW-trending Pan African shear-zone fabrics in the crystalline basement of the Sinai – African plate. Earliest syn-rift sediments are upper Oligocene continental clastic deposits with minor syn-rift basalts (**Khalil and McClay, 2001**).

The elemental compositions of the Tertiary tholeiitic and alkaline rocks have narrow ranges for SiO_2, CaO, MgO, K_2O and Na_2O. The change from the tholeiitic to alkaline character in space and time suggests that volcanism had migrated from an oceanic crust environment (Cairo-Suez Road in the N.E.

Egypt) to a continental crust environment (Bahariya Oasis in the S.W. Egypt; **Abdel-Monem and Heikel, 1981**). The alkali olivine basaltic and the tholeiitic types of magma may have evolved near a converging plate margin, the former type erupting over a continental crust and the latter erupting over an over an oceanic crust. These two types of magma dominate the volcanic activity on both sides of the southern Red Sea region (**Coleman *et al.*, 1977**).

The mid-Tertiary volcanic rocks occur as scattered out crops in several localities. The biggest two out crops of basaltic rocks are Gabal El-Yahmum at northwest part of the study district and the second out crop is Naqb Ghul (Northern Galala plateau) in the south part of the study district. The geological succession of Oligocene rocks in the study district consists from top to bottom basaltic sheet cap about 17m thick underlain by several layers of sands and sandstone.

Ni and Zr abundances in basaltic magmas formed by different extents of partial melting and fractional crystallization were modelled using mass balance equations (**Hanson, 1978**). Low extents of partial melting (up to 20%) of primitive mantle with 2000 ppm Ni and 7.8 ppm Zr will result tholeiitic magma having about 82-194 ppm Ni (**Rajamani *et al.*, 1985**). Whereas, North Eastern Desert basaltic group have 24-150 ppm Ni and hence they may not represent magma derived from the partial melting of the primitive mantle. Samples of the North Eastern Desert basaltic group show a wide variation in Zr and Ni contents. This variation could be explained as a result of different extents of partial melting of a mixed source.

In the altered basaltic dykes that cut Tertiary basalt at the Yahmum, Naqb Ghul and Wadi Qattamiya eruptions, metasomatic alteration involving small scale mobilization of Ca and Fe led to extensive replacement of the basalt by ferroaugite together with lesser amounts of calcite, quartz, montmorillonite, chlorite and gypsum.

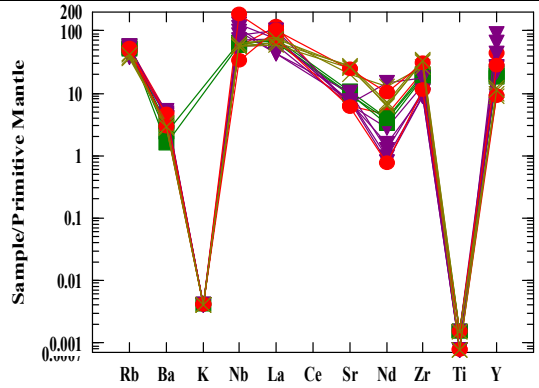

a. Primitive mantle normalized (**McDonough and Sun 1995**) trace element plots of representative basaltic rocks.

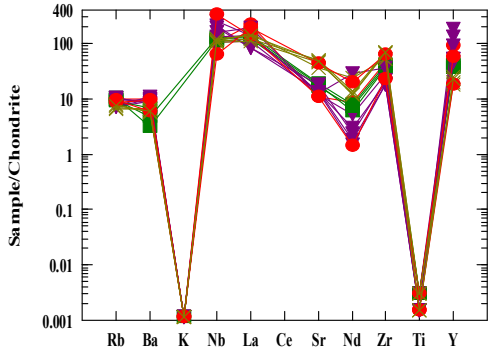

b. Chondrite normalized (**McDonough and Sun 1995**) trace element plots of representative basaltic rocks.

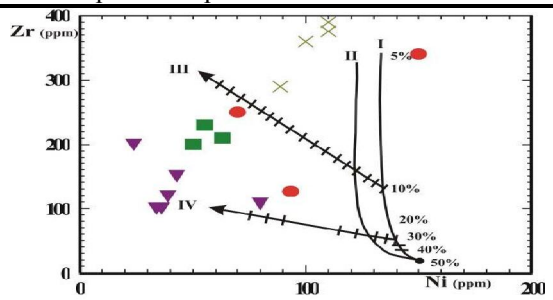

c. Trace elements modelling based on Zr versus Ni **(Rajamani *et al.*, 1985)**. I and II: Calculated batch melting curves at 1,850C, 50kb and 1,575C, 25 kb respectively, and are marked with percentage of melting. III and IV: olivine fractionation trends at one atmosphere with ticks, marking increments of 5% olivine fraction from previous tick. Values for the mantle source (7.8 ppm Zr and 2,000 ppm Ni) are taken from **Taylor and McLennan (1981)**, (source mode: 55% ol, 25% opx and 20% cpx; melting mode: 20% ol, 25% opx, 55% cpx).

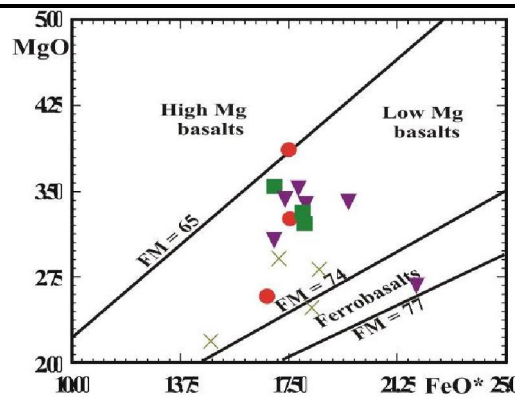

d. MgO-FeO* diagram illustrating the compositional range of the rocks. Discriminant FM ratios and basalt fields are from **Wood (1978).**

Fig.16 (a-d). Geochemical diagrams showing the petrogenesis of the studied basalts Symbols as in Fig.11a.

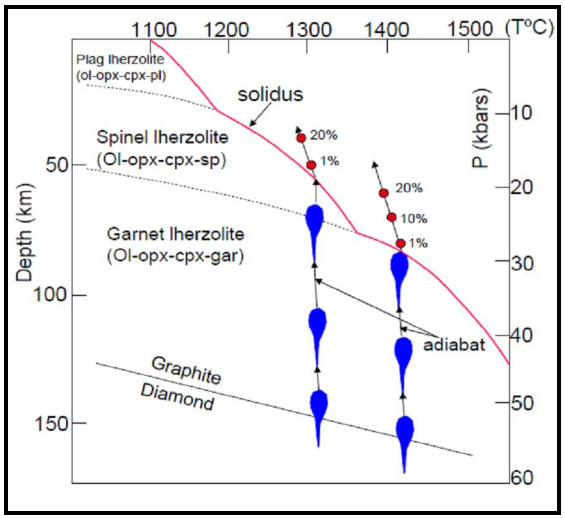

Fig.17. Melting begins when upwelling mantle intersects the peridotite solidus (**Thompson, R.N., 1972**).

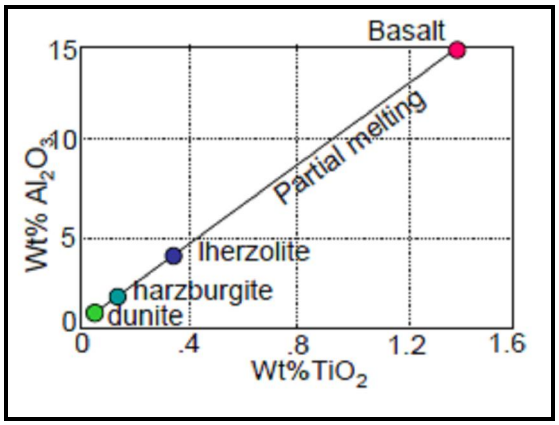

Fig.18. Partial melting (~15%) of fertile lherzolite produces basalt leaving depleted residue of harzburgite + dunite (**Thompson, R.N., 1972**).

This Ca-Fe silicate alteration is localized around leucocratic segregations in the basalts. Geochemical data indicate that the fluids responsible were meteoric and derived from the surrounding basalt-hosted hydrothermal system.

Iron-titanium oxide phenocrysts are present in some of the rocks, but they are everywhere more than 2% by volume. In many cases the opaque grains enclosed in silicate phenocrysts or aggregates of phenocrysts. Variation in chemical composition in progressively increasingly basaltic rocks includes increases in MgO, Fe_2O_3, FeO, CaO, TiO_2, Al_2O_3, Ni, Cr, Co, V, Ga, Zr and Zn, and decreases in SO_3, P_2O_5, SiO_2, Na_2O, K_2O, MnO, Cl, and Sr. Cu , Nb, Pb, and Y fluctuate.

The widespread mid Tertiary volcanic activity at central and northern Egypt have been studied geochemically by a number of authors and concluded that these volcanic rocks range from per-aluminous, meta-aluminous to tholeiitic as well as alkaline.

Conclusions

The results of the geochemistry indicate that the basaltic flows are alkali-olivine basalts (continental basalts) which formed in rift environments in Oligo-Miocene age. Continental tholeiites (within plate) considered the principal volcanic rocks generated in rift environment by mantle plume give rise tholeiites.

The immobile elemental abundances of the basalts plotted on the tectonic discrimination diagrams. Extensive volcanism in the northern Eastern Desert is probably linked with initial stages of rifting extension triggered by rising mantle plume with in Late Oligocene-Miocene age of the Egypt.

The geochemical composition of the basaltic rocks indicates that they originated in the Gulf of Suez rift setting. The type of extensional regime inferred from geochemical parameter. These rocks display geochemical features of within continental plate basalt.

The basaltic rocks sampled in the studied district are continental tholeiite and alkaline basaltic rocks emplaced on a Phanerozoic basement. The basalt lavas represent alkaline and tholeiitic magmas marking a continental rift. The maturity reached by this continental rift can be inferred using immobile trace element compositions. Our data suggest that these basaltic rocks emplaced in a Gulf of Suez Rift Basin. Basaltic rock associations above the tectonic units mark a progressive opening from a pre-rift continental break-up up to a continental rift.

The variation in altered basalt chemistry is best seen in the two samples from Gabal El-Yahmum area. The percent of SiO_2, Fe_2O_3, and CaO all increase, whereas K_2O, Na_2O, MgO, and MnO decrease, and TiO_2 remain constant. Total iron percentage fluctuates, but the iron is increasingly oxidized to Fe_2O_3.

The hot spot activity due to which wide spread volcanism took place appears to have started at Gulf of Suez Rift. The basaltic flows rest over clastic sediments and the basalt flood associated with hot water springs "hydrothermal solutions" (geysers) which penetrated of these beds where making contact aureole.

References

1. Abdel Aal, A.Y., 1981. Comparative petrological and geochemical studies of post-Cambrian basaltic rocks in Egypt: Ph.D. Thesis, Faculty of Science, El-Minia University.
2. Abdel Aal, A.Y., 1998. Mineral and chemical composition of basalts in the neighbourhood of Giza, Egypt. *Journal of African Earth Sciences,* Vol. *26,* No. 1, pp. 101 – 117.

3. Abdel-Monem, A.A., Heikel, M.A., 1981. Major element composition, magma type and tectonic environment of the Mesozoic to recent basalts, Egypt: A review. Bull. Faci. Earth Sci., K.A.U., Vol. 4, 121-148p. Faculty of Earth Sciences, King Abdulaziz University, Jeddah, Kingdom of Saudi Arabia.
4. Al-Malabeh, A., 1993. The volcanology, mineralogy and geochemistry of selected pyroclastic cones from NE-Jordan and their evaluation for possible industrial applications. Ph.D. thesis, Erlanger, Germany
5. Atia, M.S., 1978. Mineralogy and geochemistry of some basalt occurrences in Egypt: Ph.D. Thesis, Faculty of Science, Mansoura University.
6. Bogatikov, O.A., Gonshakova, V.I., Efremova, *et al*., 1981. Classification, Nomenclature and Chemical Characteristics of Igneous Rocks. The Geol. Soc. of Egypt. Translation Series. No.1. translated by Magdy M. Khalil. Revised by M.F. El-Ramly, 1994. p. 19-20.
7. Campbell, I.H., 1985. The difference between oceanic and continental tholeiites: a fluid dynamic explanation. Contrib. Miner. Petrol. 91, 37–43.
8. Chandrasekharam, D., Parthasarathy, A., 1978. Geochemical and tectonic studies on the coastal and inland Deccan trap volcanics and a model for the evolution of Deccan trap volcanism. N. Jb. Min. Abh. 132:214–229.
9. Church, B.N., 1975. Quantitative classification and chemical comparison of common volcanic rocks. *Geol. Soc. Amer. Bull.,* 86: 257-263.
10. Coffin, M.F., Eldholm, O., 1994. Large igneous provinces: Crustal structure, dimensions, and external consequences, Rev. Geophys., 32, 1–36.
11. Coleman, R.G., Fleck, R.J., Hedge, C.E., Ghent, E.D., 1977. The volcanic rocks southwest Saudi Arabia and the opening of the Red Sea. In Red Sea Research 1970-1975. Saudi Arabian Dir. Gen. Mineral Resources Bull. 22, 30p.
12. Condie, K.C., Bobrow, D.J., Card, K.D., 1987. Geochemistry of Precambrian mafic dykes from the southern Superior Province of the Canadian Shield. Geol. Assoc. Can., Spec. Pap., 34: 95-108.
13. Conoco, C., 1987. Geological map of Egypt. Scale 1: 500 000, sheet Cairo.
14. Cox, K.G., Bell, J.D., Pankhurst, R.J., 1979. The interpretation of igneous rocks. George Allen & Unwin, London.
15. Cox, K.G., Hawkesworth, C.J., 1985. Geochemical stratigraphy of the Deccan traps at Mahabaleshwar Western Ghats, India with implication for open system magmatic processes. J. Petrol. 26, 355–377.
16. El-Ashkar, A.A.A., 2002. Studies on mineralogical, geochemical and physical characteristics on basalts of Cairo-Suez road for evaluation for using in cement industry. B.Sc. Thesis, Faculty of Science, El-Azhar University, p. 12-20.
17. El-Hinnawi, E.E., Abdel Maksoud, M.A., 1972. Geochemistry of Egyptian Cenozoic basaltic rocks. Chemie der Erde, 31: 93-112.
18. Fawcett, J.J., 1965. Alteration products of olivine and pyroxene in basalt lavas from the Isle of Mull. Mineralogical Magazine, 35, 55-68.
19. Floyd, P.A., Winchester, J.A., 1975. Magma type and tectonic setting discrimination using immobile elements. *Earth Planet. Sci. Lett.* 27: 211-218.
20. Foley, E.J., 1941. Geological survey of the Cairo-Suez district and adjoining area. Standard oil Co. of Egypt S.A., unpublished internal report, No. 15, 45pp.
21. George, A., 1985. The origin of metavolcanic and associated argillaceous rocks at island bay, Wellington, *New Zealand Jour. Geol. Geophys.* 28: 623-634.
22. Hanson, G.N., 1978. The application of trace elements to the petrogenesis of igneous rocks of granitic composition; *Earth and Planetary Science Letters*. 38 26-43.
23. Holbrook, W.S., Kelemen, P.B., 1993. Large igneous province on the US Atlantic margin and implications for magmatism during continental breakup, Nature, 364, 433–436.
24. Irvine, T.N., Baragar, W.R.A., 1971. A guide to the chemical classification of the common volcanic rocks. Can. J. Earth. Sci. 8: 523-548.
25. Issawi, B., El-Hennawi, M., Mazhar, A., 1999. The Phanerozoic geology of Egypt: A geodynamic approach. Geol. Surv. Egypt. Special published No. 76, 462pp.
26. Jakobssonet, S.P., Jonsson, J., Shido, F., 1978. Journal of petrology. Vol. 19. pp. 669-705.
27. Keir, D., Bastow, I.D., Pagli, C., Chambers, E.L., 2013. The development of extension and magmatism in the Red Sea rift of Afar. Tectonophysics 607 (2013) 98–114.
28. Khalil, S.M., McClay, K.R., 2001. Tectonic evolution of the NW Red Sea – Gulf of Suez rift system. In: Wilson, R.C.L., Whitmarsh, R.B., Taylor, B. & Froitzheim, N., 2001. Non-volcanic Rifting of Continental Margins: A Comparison of Evidence from Land and Sea. Geological Society. London. Special Publications, 187, 453-473.
29. Knoper, MW., Condie. K.C., 1988. Geochemistry and petrogenesis of Early Proterozoic amphibolites. West-central Colorado. Chem. Geol., 67: 209—225.
30. Kuno, H., 1966. Lateral variations of basalt magma types across continental margins and island arcs. Bull. Volcan. XXIX, 195-222.
31. Kuno, H., 1968. Differentiation of basalt magmas. In: *Basalt: The Poldervaart, treatise on rocks of basaltic composition* 2 (Edited by Hess, H. H. and Poldervaart, A.) pp. 623-688. Interscience, New York.
32. Le Maitre, R.W., 2002. Igneous rocks, a classification and glossary of terms. (Recommendations of the International Union of Geological Sciences Subcommission on the Systematics of Igneous Rocks). Cambridge University Press, Cambridge, p 236.
33. Lutz, B.G., 1980. Geochemistry of oceanic and continental magmatism. *Moscow: Nedra* (in Russian), pp l9-26.
34. McDonough, W.F., Sun, S., 1995. The Composition of the earth. *Chem. Geol.* 120: 223-253.
35. Meneisy, M.Y., Abdel Aal, A.Y., 1983. Geochronology of Phanerozoic volcanic activity in Egypt. Ain Shams Science Bulletin, 24, pp. 163-175.

36. Meneisy, M.Y., Kreuzer, Hans, 1974. Potassium-argon ages of Egyptian basaltic rocks. Geol. Jb. *Hannover*, D9, 21-31.
37. Middlemost, E.AK, 1975. The basalt clan. Earth Sci. Rev., Vol. 11, p. 337-364.
38. Middlemost, E.A.K., 1980. A contribution to the nomenclature and classification of volcanic rocks. Geol. Mag., Vol. 117, p. 51-57.
39. Middlemost, E.A.K., 1985. Magmas and magmatic rocks-An introduction to igneous petrology. Longman, London and New York. p. 98.
40. Mohr, P.A., 1987. Crustal contamination in mafic sheets: a summary. In: Halls, H., Fahrig, W.F. (Eds.), Mafic Dyke Swarms. Geological Association of Canada Special Paper 34, pp. 75–80.
41. Patton, T.L., Moustafa, A.R., Nelson, R.A., Abdine, S.A., 1994. Tectonic Evolution and Structural Setting of the Suez Rift. In: Landon, S.M. (Ed.), Interior Rift Basins. American Association of Petroleum Geologists Memoir 59, 9-55.
42. Pearce, J.A., Cann, J.R., 1973. Tectonic setting of basic volcanic rocks determined using trace element analysis. *Earth. Planet. Sci. Lett.* 19: 290-300.
43. Pearce, J.A., Gale, G.H., 1977. Identification of ore-deposition environment from trace element geochemistry of associated igneous host rocks. In: Volcanic processes in ore genesis. Inst. Min. Metall. Geol Soc. Lond. Spec. Publ. 7:14–24.
44. Pearce, T.H., Gorman, B.E., Birkett, T.C., 1975. The TiO_2-K_2O-P_2O_5 diagram: a method of discriminating between oceanic and non-oceanic basalts. Earth Planet Sci. Lett. 24: 419-426.
45. Pearce, T.H., Gorman, B.E., Birkett, T.C., 1977. The relationship between major element chemistry and tectonic environment of basic and intermediate volcanic rocks. *Earth, Planet. Sci. Lett*. 36: 121-132.
46. Pearce, J.A., Norry, M.J., 1979. Petrogenetic implication of Ti, Zr, Y and Nb variations in volcanic rocks. *Contrib. Mineral. Petrol.* 69: 33-47.
47. Rajamani, V., Shivkumar, K., Hanson, G.N., Shirey, S.B., 1985. Geochemistry and petrogenesis of amphibolites, Kolar schist belt, South India: evidence for komatiitic magma derived by low percentages of melting of the mantle. J Petrol 26:92–123
48. Rickwood, P.C., 1989. Boundary lines within petrologic diagrams, which use oxides of major and minor elements. *Lithos*, 22: 247-263.
49. Said, R., 1962, The Geology of Egypt. Elsevier Publishing CO., Amsterdam-New York, 557p.
50. Shervais, J.W., 1982. Ti-V plots and the petrogenesis of modern and ophiolitic lavas. *Earth Planetary Science Letters* 59, 100-118.
51. Shukri, N.M., Akmal, M.G., 1953. Geology of Gebel El-Nasuri and Gebel El-Anqabya District, Bull. Soc., Egypt, Vol. 26, pp. 243-276.
52. Sigvaldson, E.E., 1974. Journal of petrology. Vol. 15, pp.497-523.
53. Sobolev, A.V., Hofmann, A.W., Kuzmin, D.V., Yaxley, G.M., Arndt, N.T., Chung, S.L., Danyushevsky, L.V., Elliott, T., Frey, F.A., Garcia, M.O., Gurenko, A.A., Kamenetsky, V.S., Kerr, A.C., Krivolutskaya, N.A., Matvienkov, V.V., Nikogosian, I.K., Rocholl, A., Sigurdsson, I.A., Sushchevskaya, N.M., Teklay, M., 2007. The amount of recycled crust in sources of mantle-derived melts. Science, Vol. 316, pp. 412–417.
54. Srivastava, R.K., 2006. Precambrian mafic dyke swarms from the central Indian Bastar craton: Temporal evolution of the subcontinental mantle. Dyke Swarms - Time Markers of Crustal Evolution-Hansk, Mertanen, Rāmō & Vuollo (eds) © 2006 Taylor & Francis Group, London.
55. Tarney, J., Weaver, B.L., 1987. Geochemistry and petrogenesis of early Proterozoic dyke swarms. In: Halls, H., Fahrig, W.F. (Eds.), Mafic Dyke Swarms. Geological Association of Canada Special Paper 34, pp. 81–94.
56. Taylor, S.R., McLennan, S.M., 1981. The Composition and Evolution of the Continental-Crust - Rare-Earth Element Evidence from Sedimentary-Rocks. Philosophical Transactions of the Royal Society of London 301(1461): 381-399.
57. Tegyey, M., 1974. Essai d'informatique pétrographique; constitution d'un fichier et application á l'étude des roches volcaniques des zones orogéniques. Thèse 3e cycles. Université d'Orléans, France, 146p.
58. Thompson, R.N., 1972. The 1-atmosphere melting patterns of some basaltic volcanic series: American Journal of Science, Vol. 272, p. 901-932.
59. Tosson, S., 1964. The volcanic rocks of Bahariya Oasis, Egypt. Bull. Volcanologique, XXVII, 447pp.
60. White, R., McKenzie, D., 1989. Magmatism at rift zones: The generation of volcanic continental margins and flood basalts. Journal of Geophysical Research: Volume 94, Issue B6, pages 7685–7729, 10 June 1989.
61. Williams, H., Turner, F.J., Gilbert, C.M., 1985. Petrography: An introduction of the study of rocks in thin sections. 2nd (ed.). pp. 96-103.
62. Winchester, J.A., Floyd, P.A., 1976. Geochemical magma type discrimination; application to altered and metamorphosed basic igneous rocks. *Earth Planet*. Sci. Lett., 28, 459-469.
63. Wood, D.A., 1978. Major and trace element variations in the Tertiary lavas of eastern Iceland and their significance with respect to the Iceland Geochemical Anomaly. *Journal Petrology* 19, 393-436.
64. Yoder, H.S., 1976. Generation of basaltic magma, US National Academy of Sciences, Washington, DC, USA.

5/28/2015